



**Carlos Filipe
Conceição Marques**

**Tratamento de Efluentes Aquosos Contaminados
com Líquidos Iónicos**

**Treatment of Aqueous Effluents Contaminated with
Ionic Liquids**



**Carlos Filipe
Conceição Marques**

**Tratamento de Efluentes Aquosos Contaminados
com Líquidos Iónicos**

**Treatment of Aqueous Effluents Contaminated with
Ionic Liquids**

Dissertação apresentada à Universidade de Aveiro para cumprimento dos requisitos necessários à obtenção do grau de Mestre em Engenharia Química, realizada sob a orientação científica do Prof. Dr. João Manuel da Costa Araújo Pereira Coutinho, Professor Associado com agregação do Departamento de Química da Universidade de Aveiro, e co-orientação da Dr^a. Mara Guadalupe Freire Martins, Estagiária de Pós-Doutoramento do Instituto de Tecnologia Química e Biológica, ITQB2, Universidade Nova de Lisboa.

...à minha mãe e sobrinhas.

o júri

presidente

Prof^a. Dr^a. Maria Inês Purcell de Portugal Branco
professora auxiliar do Departamento de Química da Universidade de Aveiro

Prof. Dr. João Manuel da Costa e Araújo Pereira Coutinho
professor associado com agregação do Departamento de Química da Universidade de Aveiro

Dr^a. Ana Belén Pereiro Estévez
investigadora Marie Curie do Instituto de Tecnologia Química e Biológica, ITQB2, da Universidade Nova de Lisboa

Dr^a. Mara Guadalupe Freire Martins
estagiária de pós-doutoramento do Instituto de Tecnologia Química e Biológica, ITQB2, da Universidade Nova de Lisboa

agradecimentos

As minhas primeiras palavras vão para o professor João Coutinho, por ter acreditado em mim, e me ajudar em todos os aspetos inerentes a este trabalho.

Seguidamente quero agradecer à Mara Freire e à Catarina Neves pelo seu acompanhamento diário e paciência para comigo.

Ao grupo PAtH pela boa disposição, companheirismo, ajuda, socialização e sorrisos que me proporcionaram ao longo deste ano.

À Cristiana Cruz, Cátia Sousa, Susete Correia e Vânia Martins por todas as conversas, troca de opiniões, lazer, diversão e amizade.

Por fim mas não menos importantes a todos os meus amigos que me acompanharam ao longo destes anos.

palavras-chave

Líquidos iônicos, tratamento de efluentes aquosos, recuperação, adsorção, sistemas aquosos bifásicos, carvão ativado, sais de sódio

resumo

Este trabalho visa o tratamento de efluentes aquosos contaminados com líquidos iônicos (LIs).

Os LIs são sais que a temperaturas inferiores a 373 K e à pressão atmosférica permanecem no estado líquido. Isto deve-se ao tamanho e assimetria dos íons envolvidos na composição dos LIs que os faz apresentar propriedades distintas dos sais convencionais. Dado a serem compostos por íons, os LIs podem ser sintetizados consoante uma determinada finalidade e/ou propriedades necessárias para uma aplicação específica. Por apresentarem pressões de vapor desprezáveis, estes não poluem a atmosfera e têm sido, por isso, considerados solventes menos agressivos para o meio ambiente. No entanto, estes compostos apresentam uma solubilidade não desprezável em água, o que por outro lado, pode conduzir à poluição de efluentes aquosos quando se antecipa, num futuro próximo, o uso destes solventes à escala industrial.

Neste trabalho foram estudados dois processos de remoção e recuperação de LIs de fases aquosas: adsorção (para o caso de LIs hidrofóbicos, e logo, pouco solúveis em água e com uma concentração baixa nos efluentes aquosos); e sistemas aquosos bifásicos (para os LIs hidrofílicos, miscíveis com água, e que apresentam concentrações mais elevadas nos efluentes aquosos). Para o estudo do processo de adsorção o adsorvente usado foi o carvão ativado, à temperatura de 308.0 K e à pressão atmosférica. Os resultados obtidos mostram que os LIs hidrofóbicos podem ser removidos de efluentes aquosos por adsorção. O processo fundamentado em sistemas aquosos bifásicos foi estudado à temperatura de 298 K e à pressão atmosférica utilizando como sal comum o Na_2CO_3 . As eficiências de recuperação dos diversos LIs foram sempre superiores a 90 %.

keywords

Ionic liquids, treatment of aqueous effluents, recovery, adsorption, aqueous biphasic systems, activated charcoal, sodium-based salts

abstract

This work aims the treatment of aqueous effluents contaminated with Ionic Liquids (ILs).

ILs are salts that remain liquid at temperatures lower than 373 K and at atmospheric pressure due to the size and asymmetry of the ions involved in the IL composition, and which allow them to present different melting temperatures when compared with conventional salts. Since ILs are exclusively composed of ions, they can be prepared according to a given application and/or with designed properties. ILs present negligible vapour pressures, and thus, they do not contribute to atmospheric pollution. Hence, based on this property, ILs have been considered new solvents with less hazardous characteristics to the environment. Nevertheless, ILs display a non-negligible solubility in water which could lead, on the other hand, to the contamination of aqueous effluents, especially when the large-scale application of these solvents is envisaged in a near future. In this work, two processes for the separation and recovery of ILs from aqueous phases were studied: adsorption (for hydrophobic ILs that present a low solubility in water and therefore a low concentration in aqueous effluents); and aqueous biphasic systems (for hydrophilic ILs which are miscible with water and present higher concentrations in the aqueous streams).

For the adsorption process, activated charcoal was studied as the main adsorbent, at 308.0 K and atmospheric pressure. The gathered results indicate that hydrophobic ILs can be removed from aqueous effluents by adsorption. For the process based on aqueous biphasic systems, the studies were conducted at 298 K and atmospheric pressure, and making use of a common salt – Na_2CO_3 . The recovery efficiencies of all ILs were always higher than 90 %.

Contents

Contents	xv
List of Symbols	xvii
List of Abbreviations	xix
List of Tables	xxiii
List of Figures	1
1 General Introduction	Erro! Marcador não definido.
1.1 General Context	Erro! Marcador não definido.
1.2 Scope and objectives.....	Erro! Marcador não definido.
2 Adsorption of ILs into Activated Charcoal	Erro! Marcador não definido.
2.1 Introduction.....	Erro! Marcador não definido.
2.2 Experimental Section.....	Erro! Marcador não definido.
2.3 Results and Discussion	Erro! Marcador não definido.
2.4 Conclusions.....	Erro! Marcador não definido.
3 Recovery of ILs using Aqueous Biphasic Systems	27
3.1 Introduction.....	Erro! Marcador não definido.
3.2 Experimental Section.....	Erro! Marcador não definido.
3.3 Results and Discussion	Erro! Marcador não definido.
3.4 Conclusions.....	Erro! Marcador não definido.
4 Final Remarks	39
4.1 Future Work.....	Erro! Marcador não definido.
5 References	43
5.1 References:.....	Erro! Marcador não definido.
Appendix	51

Appendix A.....	Erro! Marcador não definido.
Appendix B.....	Erro! Marcador não definido.

List of Symbols

$\% R$	Recovery efficiency percentage
$[\text{IL}]_B$	IL weight fraction percentage in the bottom phase
$[\text{IL}]_M$	IL weight fraction percentage in the mixture
$[\text{IL}]_T$	IL weight fraction percentage in the top phase
$[\text{Salt}]_B$	Salt weight fraction percentage in the bottom phase
$[\text{Salt}]_M$	Salt weight fraction percentage in the mixture
$[\text{Salt}]_T$	Salt weight fraction percentage in the top phase
A, B, C	Fitted parameters of the Merchuck equation
C_e	Concentration of IL in equilibrium in the liquid phase
C_i	Initial concentration of IL in the liquid phase
K_d	Coefficient of apparent distribution
K_f	Empirical coefficient of Freundlich
L	Ratio of adsorption-desorption constants
n	Empirical coefficient of Freundlich
q_e	Concentration of IL in equilibrium in the solid phase
q_{\max}	Maximum concentration of IL in the adsorbent
V	Total volume of the solution in equilibrium

List of Abbreviations

Cations

$[\text{aC}_1\text{im}]^+$	1-allyl-3-methylimidazolium cation
$[\text{C}_1\text{C}_1\text{im}]^+$	1,3-dimethylimidazolium cation
$[\text{C}_2\text{C}_1\text{im}]^+$	1-ethyl-3-methylimidazolium cation
$[\text{C}_2\text{C}_2\text{im}]^+$	1,3-diethylimidazolium cation
$[\text{C}_2\text{C}_3\text{im}]^+$	1-ethyl-3-propylimidazolium cation
$[\text{C}_2\text{im}]^+$	ethylimidazolium cation
$[\text{C}_3\text{C}_1\text{im}]^+$	1-propyl-3-methylimidazolium cation
$[\text{C}_3\text{C}_3\text{im}]^+$	1,3-dipropylimidazolium
$[\text{C}_4\text{-2-C}_1\text{py}]^+$	1-butyl-2-methylpyridinium cation
$[\text{C}_4\text{-3-C}_1\text{py}]^+$	1-butyl-3-methylpyridinium cation
$[\text{C}_4\text{-4-C}_1\text{py}]^+$	1-butyl-4-methylpyridinium cation
$[\text{C}_4\text{C}_1\text{im}]^+$	1-butyl-3-methylimidazolium cation
$[\text{C}_4\text{C}_1\text{pip}]^+$	1-butyl-3-methylpiperidinium cation
$[\text{C}_4\text{C}_1\text{pyr}]^+$	1-butyl-1-methylpyrrolidinium cation
$[\text{C}_4\text{py}]^+$	1-butylpyridinium cation
$[\text{C}_5\text{C}_1\text{im}]^+$	1-pentyl-3-methylimidazolium cation
$[\text{C}_6\text{C}_1\text{im}]^+$	1-hexyl-3-methylimidazolium cation
$[\text{C}_n\text{C}_1\text{im}]^+$	1- alkyl-3-methylimidazolium cation
$[\text{N}_{2\text{HHH}}]^+$	ethylammonium cation
$[\text{N}_{4444}]^+$	tetrabutylammonium cation
$[\text{P}_{4444}]^+$	tetrabutylphosphonium cation

Anions

$[\text{BF}_4]^-$	tetrafluoroborate anion
$[\text{C}(\text{CN})_3]^-$	tricyanomethane anion
$[\text{C}_2\text{H}_5\text{SO}_3]^-$	ethylsulfate anion
$[\text{CF}_3\text{CO}_2]^-$	trifluoroacetate anion
$[\text{CF}_3\text{SO}_3]^-$	trifluoromethanesulfonate (triflate) anion
$[\text{CH}_3\text{CO}_2]^-$	acetate anion
$[\text{CH}_3\text{SO}_4]^-$	methylsulfate anion
$[\text{DMP}]^-$	dimethylphosphate anion
$[\text{FAP}]^-$	tris(perfluoroalkyl)trifluorophosphate anion
$[\text{N}(\text{CN})_2]^-$	dicyanamide anion
$[\text{NTf}_2]^-$	bis(trifluoromethylsulfonyl)amide anion
$[\text{PF}_6]^-$	hexafluorophosphate anion
$[\text{SCN}]^-$	thiocyanate anion
$[\text{Tos}]^-$	4-methylbenzenesulfonate (tosylate) anion
Br^-	bromide anion
Cl^-	chloride anion

Acronyms

A_{BET}	BET area
ABS	Aqueous Biphasic Systems
AC	Activated Charcoal
A_{ext}	External area
GAC	Granular Activated Charcoal
ILs	Ionic Liquids
M_w	Molecular weight fraction
RTILs	Room temperature Ionic Liquids
Si/Al	Siliceous-aluminium ratio
TL	Tie-Line
TLL	Tie-Line Length
V_{micro}	Micropore volume
VOCs	Volatile Organic Compounds

List of Tables

Table 1 - Summarized properties of ILs [2]. **Erro! Marcador não definido.**

Table 2 - Log(EC₅₀) values of the luminescent marine bacteria *Vibrio fischeri* after exposure to some ILs and VOCs (15 minutes)[13]. **Erro! Marcador não definido.**

Table 3 - Characterization of the GAC used in this work. ... **Erro! Marcador não definido.**

Table 4 - K_d values of the ILs studied. **Erro! Marcador não definido.**

List of Figures

Figure 1 - Some common cations and anions in IL.....**Erro! Marcador não definido.**

Figure 2 - Resume of applications of ILs in industry [2, 10, 27].**Erro! Marcador não definido.**

Figure 3 - Sample of GAC from Merck used in this work...**Erro! Marcador não definido.**

Figure 4 - Heteroatoms and groups commonly found in the AC surface [38].**Erro! Marcador não definido.**

Figure 5 - Adsorption isotherms for comparing the increase of the alkyl side chain length in ILs at 308.0 K: a), (\diamond) [C₁C₁im][NTf₂], (\blacksquare) [C₂C₁im][NTf₂], (\bullet) [C₃C₁im][NTf₂], (\blacktriangle) [C₄C₁im][NTf₂], (\blacklozenge) [C₅C₁im][NTf₂], (\times) [C₆C₁im][NTf₂]; b) ($*$) [C₂im][NTf₂], (\circ) [C₂C₂im][NTf₂], (\triangle) [C₂C₃im][NTf₂]; c), (\blacklozenge) [C₃C₃im][NTf₂], [C₂C₂im][NTf₂], (\diamond) [C₁C₁im][NTf₂].....**Erro! Marcador não definido.**

Figure 6 - Adsorption isotherms for comparing the isomeric ILs at 308.0 K: a), ($*$) [C₂im][NTf₂], (\diamond) [C₁C₁im][NTf₂]; b), (\bullet) [C₃C₁im][NTf₂], (\circ) [C₂C₂im][NTf₂]; c) (\blacktriangle) [C₄C₁im][NTf₂], (\triangle) [C₂C₃im][NTf₂], d); (\blacklozenge) [C₅C₁im][NTf₂], (\blacklozenge) [C₃C₃im][NTf₂]...**Erro! Marcador não definido.**

Figure 7 - Binodal curves for the [C₄C₁im]-based ILs at 298 K: (\times) [C₄C₁im][Tos]; (—) [C₄C₁im][CF₃SO₃]; (\diamond) [C₄C₁im][CH₃SO₄]; (\circ) [C₄C₁im][DMP]; (\square) [C₄C₁im][C₂H₅SO₄]; (\bullet) [C₄C₁im][SCN]; (\blacksquare) [C₄C₁im][N(CN)₂]; (\blacklozenge) [C₄C₁im][CH₃SO₃]; (+) [C₄C₁im]Cl; ($*$) [C₄C₁im]Br.**Erro! Marcador não definido.**

Figure 8 - Binodal curves for the Cl-based ILs at 298 K: ($*$) [C₄C₁im]Cl; (\circ) [C₄C₁pip]Cl; (\blacktriangle) [C₄-3-C₁py]Cl; (\bullet) [C₄C₁pyr]Cl; (\blacklozenge) [N₄₄₄₄]Cl; (\triangle) [P₄₄₄₄]Cl.**Erro! Marcador não definido.**

Figure 9 - Binodal curves for imidazolium-chloride-based ILs at 298 K: ($*$) [C₄C₁im]Cl; (\blacktriangle) [C₂C₁im]Cl; (\blacklozenge) [C₆C₁im]Cl; (\circ) [aC₁im]Cl.**Erro! Marcador não definido.**

Figure 10 - Binodal curves for pyridinium-based isomeric ILs at 298 K: (\blacktriangle) [C₄-3-C₁py]Cl; (\times) [C₄-4-C₁py]Cl; (\bullet) [C₄-2-C₁py]Cl; (\blacklozenge) [C₄py]Cl.**Erro! Marcador não definido.**

Figure 11 - Percentage recovery efficiency (% *R*) of ILs.....**Erro! Marcador não definido.**

Figure 12 - Scheme for the water treatment process making use of ABS.**Erro! Marcador não definido.**

1 General Introduction

1.1 General Context

Ionic liquids (ILs) can be defined as novel compounds with relatively large ions: organic cations with a low degree of symmetry, which most often involves either positively charged nitrogen-, phosphorus- or sulphur-based cations, and weakly coordinated organic or inorganic anions that mostly have a diffuse negative charge. These characteristics tend to decrease the lattice energy of the crystalline structure of the IL, and therefore to decrease their melting temperatures. ILs that are liquid at atmospheric conditions are usually identified as Room Temperature Ionic Liquids (RTILs). The first known IL was ethylammonium nitrate with a melting temperature of 13-14 °C, and discovered by Paul Walden in 1914 [1]. Yet, only in the past few decades, the interest in those compounds has been increasing both in academic and industrial fields [2, 3]. Some of the most common cations and anions that can be combined to compose a given IL are presented in **Figure 1** [2-8].

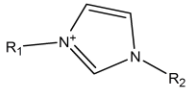
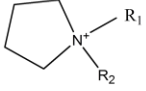
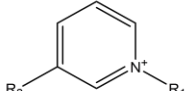
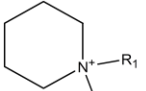
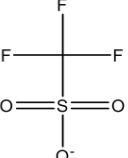
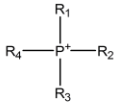

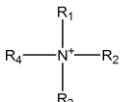
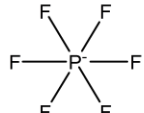
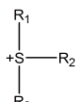
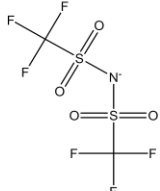
Cations		Anions	
	1-alkyl-3-alkylimidazolium [C _n C _n im] ⁺	Cl^-	chloride
	<i>N,N</i> -dialkylpyrrolidinium [C _n C _n pyr] ⁺	Br^-	bromide
	<i>N,3</i> -dialkylpyridinium [C _n -3-C _n py] ⁺	$\text{N}\equiv\text{S}^-$	thiocyanate [SCN] ⁻
	<i>N,N</i> -dialkylpiperidinium [C _n C _n pip] ⁺		triflate (trifluoromethanesulfonate) [CF ₃ SO ₃] ⁻
	tetraalkylphosphonium [P _{nnnn}] ⁺		tetrafluoroborate [BF ₄] ⁻
	tetraalkylammonium [N _{nnnn}] ⁺		hexafluorophosphate [PF ₆] ⁻
	trialkylsulfonium [S _{mmm}] ⁺		bis(trifluoromethylsulfonyl)amide [NTf ₂] ⁻

Figure 1 - Some common cations and anions in IL.

One of the major advantages, that make of ILs interesting compounds, is the possibility of combining the cation and anion in order to have a specific IL with desirable physicochemical properties for being applied in a specific task [4]. Indeed, this is the main reason behind the common “designer solvents” nomination [2]. As a relevant example of their tunable character is the solubility of imidazolium-based ILs in water, which is drastically changed, covering a range from almost immiscibility to complete miscibility with water, according to the nature of each anion [9, 10].

ILs have some unique properties, such as negligible vapor pressure, a low melting temperature, high thermal and chemical stabilities, a general non-flammability, high ionic conductivity, and a high solvating capacity for organic, inorganic, organometallic and polymeric compounds. These properties are summarized in **Table 1** [4, 9-13].

Table 1 - Summarized properties of ILs [2].

Property	ILs
Number of solvents	>1, 000,000
Applicability	Multifunction
Catalytic ability	Common and tuneable
Chirality	Common and tuneable
Vapour pressure	Negligible vapour pressure under normal conditions
Flammability	Usually nonflammable
Solvation	Strongly solvating
Tuneability	Virtually unlimited range means “designer solvents”
Cost	Typically between 2 and 100 times the cost of VOCs
Recyclability	Economic imperative
Viscosity/cP	22-40,000
Density / g·cm ⁻³	0.8-3.3
Refractive index	1.5-2.2

Volatile organic compounds (VOCs), such benzene, toluene, formaldehyde, 1,3-butadiene and dichloromethane [14], are normally used by industry in a wide range of

chemical processes, being pollutants to atmosphere and/or aqueous streams. In the environment VOCs are destroyers of the ozone layer and agents of acid rain, even at lower concentrations [15]. Moreover, they are harmful to human health, affecting the nervous system [15]. Their flammable nature also makes of them potentially explosive compounds [6, 9, 15]. In this context, ILs are a good alternative to replace VOCs, since they do not evaporate and can prevent the atmospheric pollution [4, 16]. The use of ILs as solvents has a further advantage: due to their basicity or acidity they can perform as combined solvents and catalysts, with no need of additional metal catalysts to the reaction [4].

Due to the large range of ions that can be combined, ILs can be hydrophilic or hydrophobic. Hydrophobic ILs, when mixed with water, form a second liquid phase, whereas hydrophilic ionic liquids are miscible with water at or near room temperature. It should be remarked that hydrophobic ILs are also hygroscopic, and the presence of water in ILs has important implications for the design of processes. As an example, the viscosity of ILs drastically changes with the presence of water [17, 18].

Seddon et al. [18] stated that at room temperature, all $[C_nC_{1m}][PF_6]$ are insoluble in water. The authors also found that halide- (Cl^- , Br^- , and I^-), acetate-, nitrate- and trifluoroacetate-based ILs are fully water-soluble, and ILs based on $[BF_4]^-$ and $[CF_3SO_3]^-$ anions present a miscibility with water that further depends on the alkyl side chain length in the cation. For instance, from $[C_2C_{1m}]^+$ to $[C_4C_{1m}]^+$ with the anion $[BF_4]^-$ the ILs are miscible with water while for longer alkyl side chain cations they form two phases. This fact shows that both the cation and the anion have a significant influence on the ILs water miscibility, albeit the effect of the cation is less relevant [18].

In other studies [16, 19, 20] it was possible to conclude that the hydrophobicity of cations, according to the solubility of water in ILs, increases in the following order: imidazolium < pyridinium \leq pyrrolidinium < piperidinium < phosphonium [16], whereas in the water-rich phase the solubility of the ILs increases according to: piperidinium < pyridinium < pyrrolidinium < imidazolium [19]. Moreover, an increase in the cation side alkyl chain length decreases the solubility of the ILs in water [19]. Concerning the anions, the hydrophobicity increases in the order: $[CF_3SO_3]^- < [BF_4]^- < [(C(CN)_3)]^- < [PF_6]^- < [NTf_2]^- < [FAP]^-$ [20].

Besides all the tailoring on the ILs miscibility with water it should be stressed that even the hydrophobic ILs presents a non-negligible solubility in water [21], and thus can

contaminate the aqueous effluents when used in large-scale. ILs can therefore accumulate on the environment posing some environmental risks, and aspects such as toxicity and biodegradability [4, 13] should be deeply investigated. In addition, the search of novel methods capable of removing and recovering ILs from aqueous streams is of great concern.

To evaluate the toxicity of a given IL, *Vibrio fischeri* acute tests are often carried out [13, 22, 23]. The effective concentration where the luminescence of the bacteria decreased 50 % (EC_{50}) is shown in **Table 2** for some ILs and some organic solvents. Usually this concentration is presented in a logarithm scale, and a lower $\log(EC_{50})$ corresponds to a higher level of toxicity.

Table 2 - $\log(EC_{50})$ values of the luminescent marine bacteria *Vibrio fischeri* after exposure to some ILs and VOCs (15 minutes)[13].

ILs	$\log(EC_{50} / \mu\text{M})$	VOCs	$\log(EC_{50} / \mu\text{M})$
[C ₄ C ₁ im][BF ₄]	3.55	Methanol	5.00
[C ₅ C ₁ im][BF ₄]	3.14	Acetone	4.29
[C ₆ C ₁ im][BF ₄]	2.15	Dichloromethane	3.40
[C ₇ C ₁ im][BF ₄]	2.44	Benzene	2.03
[C ₈ C ₁ im][BF ₄]	1.41	Toluene	1.50
[C ₉ C ₁ im][BF ₄]	0.72	Phenol	1.49
[C ₁₀ C ₁ im][BF ₄]	-0.18	O-Xylene	0.97
[C ₄ C ₁ im]Cl	2.95		
[C ₄ C ₁ im]Br	3.07		
[C ₄ py]Br	2.73		
[C ₄ C ₁ py]Br	2.12		
[C ₆ C ₁ py]Br	1.48		
[C ₈ C ₁ py]Br	0.25		

Generally, the toxicity of ILs increases as a function of the cation side alkyl chain length: the longer the side chain the more toxic is the IL. When comparing the $\log(EC_{50})$ values between ILs with VOCs they seem to present equivalent toxicities.

Stock et al. [24] studied the pyridinium-, imidazolium- and phosphonium-based ILs, and concluded that the toxicity of these cations increases in the order: phosphonium < imidazolium < pyridinium (acetylcholinesterase inhibition). Concerning the anion nature, it was found that it does not have an important impact on the toxicity of ILs [24]. Arning et al. [25] observed that particularly the fluoride-based anions show a significant toxicity; however, this toxic effect is lower when a hydroxyl, ether or nitrile groups are incorporated into the IL cation.

New ILs should not only present low toxicity, but also should be biodegradable to prevent their accumulation in the environment [13]. Gathergood et al. [12] concluded that amide groups in the side chain of the IL cation show poor biodegradability. On the other hand, with the increase in the alkyl side chain length, the biodegradability increases. The first biodegradable IL was found by Gathergood et al. [26], and this IL incorporated an ester group in the side chain of an imidazolium-based cation combined with the octylsulfate anion. The biodegradability, measured using CO₂ headspace tests, ranged between 60 and 67 %. A compound is considered biodegradable when it reaches 60 % of biodegradation [26].

Given the specific properties and variety of ions, ILs can be used for a large range of novel applications and are actually receiving some attention from industry [10, 12, 27]. A whole range of applications comprehends the extraction and separation processes, electrochemistry, heat transfer, analytical procedures, catalysis and synthesis, lubrication and solvents in organic synthesis. **Figure 2** summarizes the application fields of ILs [27].

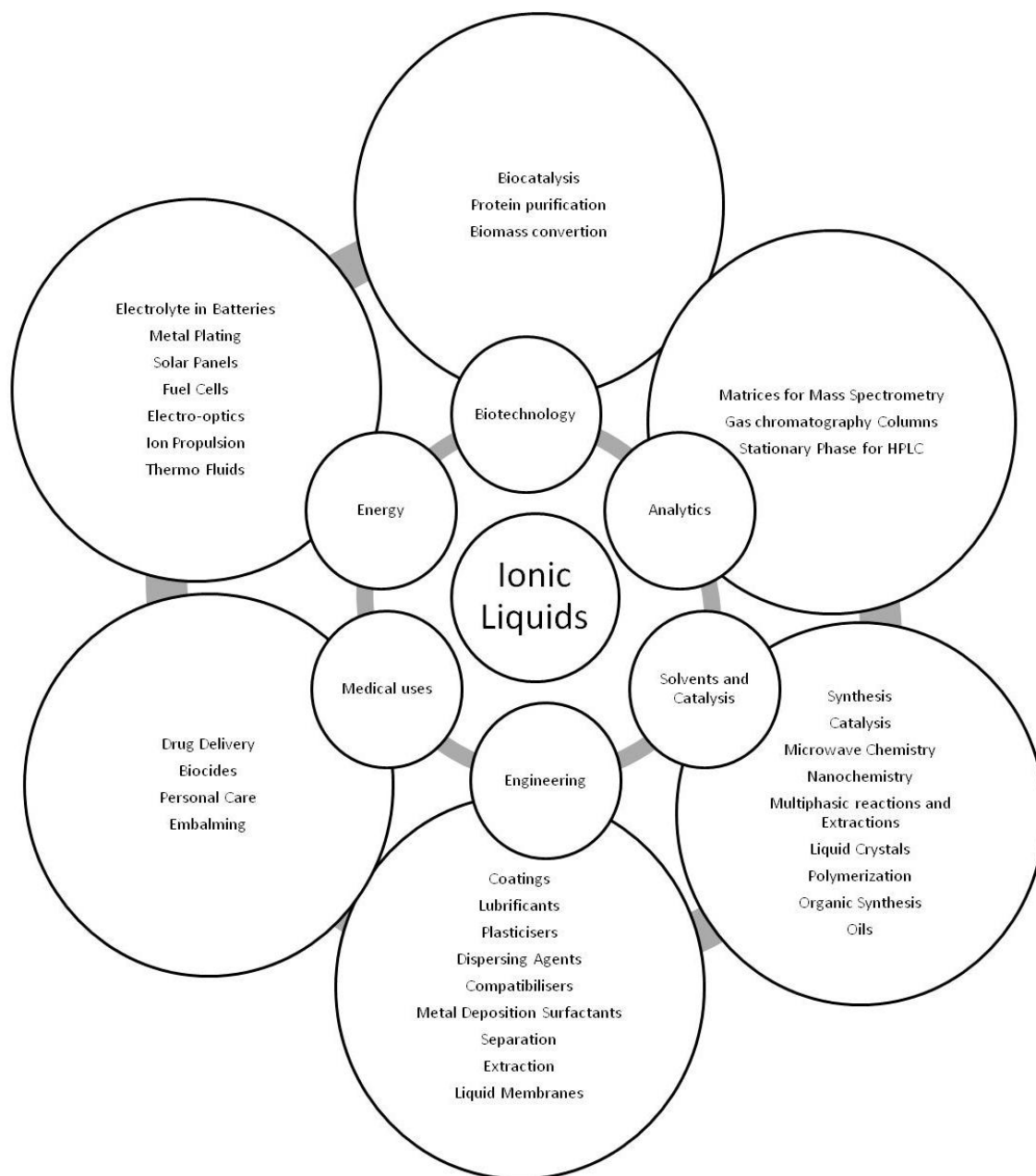


Figure 2 - Resume of applications of ILs in industry [2, 10, 27].

In fact, ILs have been already used in some industrial processes. Some companies actually use ILs as solvents, such as the "Institut Français du Pétrole" (IFP), BP, Petrochina (to perform butene's alkylation), ExxonMobil, Chevron and Chevron Philips in the petrochemical area [2]. BASF uses ILs as photoinitiator precursors, or as acid scavengers in the BASIL process [2]. IoLiTec that is a company specialized in the synthesis of ILs is developing also some interesting applications, one of which comprises the use of ILs as an

antistatic cleaning agent for value and sensitive surfaces [2]. Central Glass Co, Ltd., from Japan, produces pharmaceutical intermediates using phosphonium-based ILs [2].

The use of ILs in industrial applications [28], or just the synthesis of ILs [29], is invariably linked to water. Therefore, investigations directed to the finding of novel methods or separation processes capable of treating aqueous effluents contaminated with ILs are of crucial need.

1.2 Scope and objectives

In the coming times, a new class of solvents is emerging and have been largely classified as "greener" solvents capable of replacing the typical VOCs: Ionic Liquids (ILs). These compounds have a main advantage, namely their negligible vapour pressure which eliminate the concerns regarding the atmospheric pollution [4, 30]. Although ILs do not contribute to air pollution, their solubility in water, even for those considered hydrophobic, is non-negligible. Moreover, their toxicity and biodegradability are two vital properties that should not be discarded. The great interest in ILs and their increasing use in industrial applications will certainly lead to the discharge of ILs into aquatic ecosystems. Therefore, it is imperative to study additional separation processes to remove ILs from aqueous effluents to prevent their accumulation in the environment.

With the goal of finding novel methods for removing and recovering from aqueous media, in this work, two separation processes were investigated: adsorption making use of activated charcoal and recovery with aqueous biphasic systems (ABS). These two processes were selected to cover a wide range of concentrations of ILs that can be present in diverse aqueous effluents. It should be remarked that adsorption is particularly valuable to remove hydrophobic ILs, *i.e.*, ILs with a low concentration in water due to their low miscibility. In this work, the adsorption of several hydrophobic [NTf₂]-based ILs was studied and evaluated by their adsorption isotherms. Concerning hydrophilic ILs, and taking into account that they can be present in high concentrations in the aqueous medium, the ability to form ABS with Na₂CO₃ was here evaluated, and their recovery efficiencies determined for a large range of ILs.

2 Adsorption of ILs into Activated Charcoal

2.1 Introduction

In the past few years, several techniques and methods to remove and recover ILs from water streams have been studied. The techniques include vacuum distillation, crystallization and liquid-liquid extraction [31]. Nevertheless, all of these techniques are not suitable for removing ILs at low concentrations and are energetically expensive. In addition, thermal degradation, chemical oxidation or biological treatments have also been studied to eliminate ILs from aqueous environments; unfortunately, these methods lead to the ILs degradation and to the formation of by-products [6, 9, 28, 31-34]. An alternative method, which has already shown to be promising, consists in the adsorption of ILs onto activated charcoal [9, 31].

Adsorption is a result of unsaturated and unbalanced molecular forces that are present in a solid surface. When a solid surface is in contact with a liquid or a gas, adsorption occurs due to the interactions between the field of forces of the surface and the liquid or gas [35]. The adsorption process is classified into two types, physical adsorption and chemical adsorption, which depends on the nature of the forces that are involved between the adsorbate and the adsorbent. Physical adsorption occurs when organic molecules are held on the surface and in the pores of the adsorbent by common non-covalent interactions. Generally, this type of adsorption is usually characterized by a low heat of adsorption and by the reversible and rapidly equilibrium that can be established. On the other hand, chemical adsorption involves a chemical reaction between the adsorbate and the adsorbent [36]. The adsorption that takes place in a given adsorbate-adsorbent system depends on the nature of both, the reactivity of the surface, the surface area of the adsorbate and of adsorption conditions, such as temperature and pressure [35].

Activated Charcoal (AC), as adsorbent, has some advantages and disadvantages. Its high porosity, extended surface area, possible surface reactivity or inertness, thermal stability, and the possibility of being used in a broad pH range makes of AC a good adsorbent for several separation processes, such as in the water and air treatment/purification [35, 37]. As disadvantages, AC can be expensive and flammable in some extreme applications [36], can promote the polymerization or oxidation of some solvents to toxic or insoluble compounds [36], and some additional problems related to powdered AC and its removal from aquatic systems [35]. This type of adsorbent includes a wide range of amorphous carbonaceous materials; it can be obtained by combustion and

thermal decomposition of those materials. The granular activated charcoal (GAC), used in this work and depicted in **Figure 3**, has a large and strongly developed internal surface area and a polydisperse capillary structure comprising pores of different sizes and shapes [35].



Figure 3 - Sample of GAC from Merck used in this work.

The pores in the adsorbents are generally divided into three groups: the micropores, with diameters lower than 2 nm; mesopores, with diameters between 2 and 50 nm; and macropores, with diameters greater than 50 nm. Usually, micropores display a large surface area, about 95 % of the total area, and adsorption in these pores occurs through volume filling [35]. The adsorption energy in these pores is higher than the energy in meso and macropores, where the mesopores contribute to about 5% of the total surface area of the AC. The macropores contribution is not important since its surface area do not exceed $0.5 \text{ m}^2 \cdot \text{g}^{-1}$ [35].

The adsorption capacity of an AC is determined not only by the porous structure and size, but is also strongly influenced by the chemical structure of the carbon surface. The carbon atoms that have unpaired electrons and residual valences are richer in potential energy. These carbon atoms are highly reactive and are denominated active sites, which determine the surface reactions and catalytic reactions of carbons. Invariably, the structure of AC is associated with some heteroatoms like hydrogen, oxygen and nitrogen bonded at the edges and corners, or to the carbons atoms that are dislocated on the AC structure. The chemical structure of common ACs is shown in **Figure 4** [35].

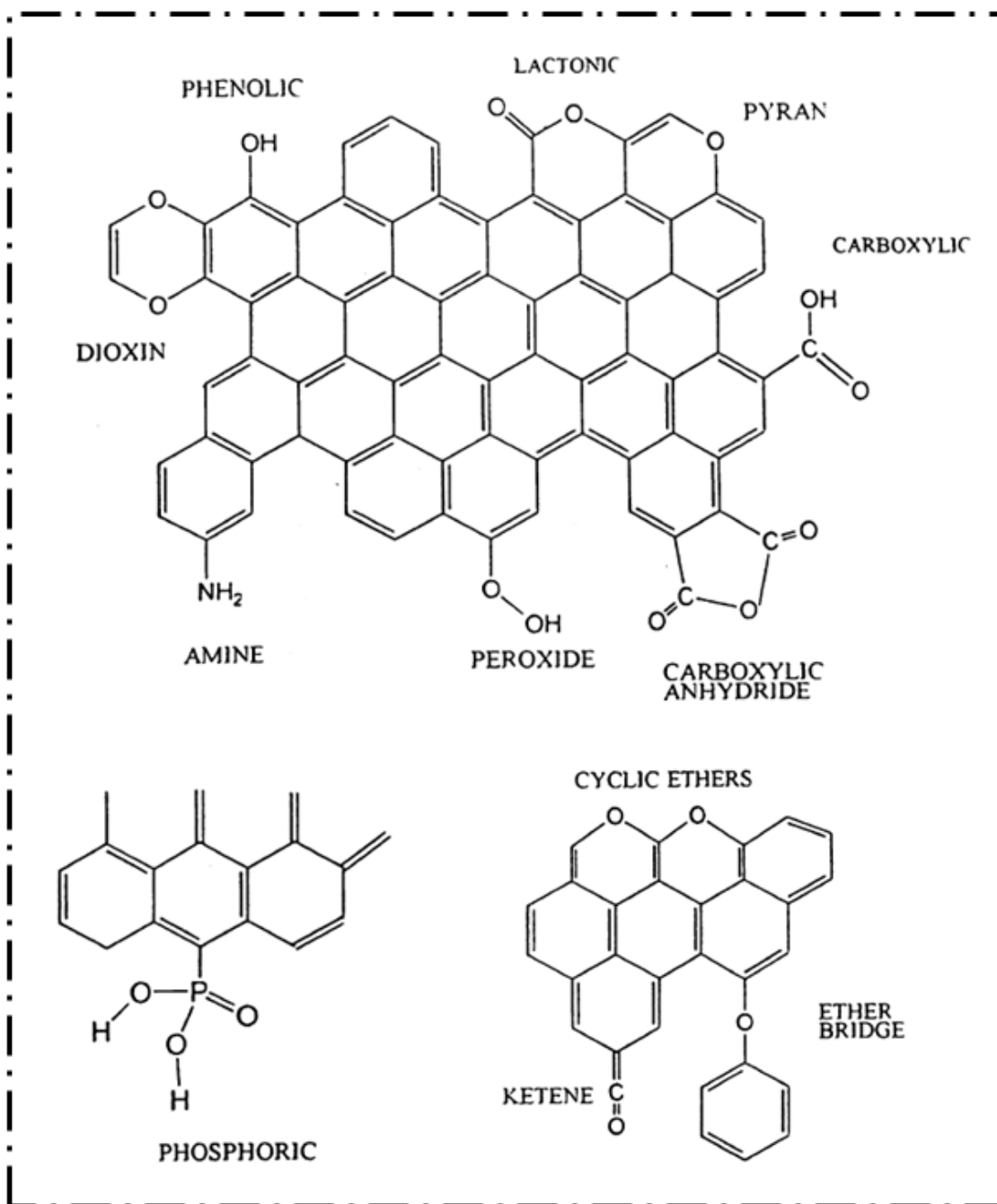


Figure 4 - Heteroatoms and groups commonly found in the AC surface [38].

Carbon-oxygen surface groups are by far the most important groups, and the oxygen content on AC can vary between 1 and 20 %. It influences the surface in their chemical characteristics in respect to hydrophobicity, which decreases with increasing the oxygen content, polarity and acidity. In fact, the presence of oxygen in the AC surface has an important effect on the adsorption capacity [35]. In order to modify, and to gather an

improved adsorption for a specific compound, ACs can be treated with sulfurization, halogenation, nitrogenation and impregnation, resulting in different kinds of surface [35].

Brennecke et al. [17] tried the adsorption of ILs into AC, and considered it as an option to treat contaminated water. The tests shown by the authors demonstrated that $[\text{C}_4\text{C}_1\text{im}][\text{PF}_6]$ can be successfully removed [17]. Palomar et al., in two recent publications [9, 31], studied the adsorption of 27 ILs into AC and modified AC by oxidative and thermal treatments, and with two inorganic adsorbents. In these works the authors also proposed a regenerating procedure for the AC and recovery of the IL with acetone extraction [9, 31].

2.2 Experimental Section

2.2.1 Materials

In this work, the adsorption isotherms were studied for several bis(trifluoromethylsulfonyl)amide- $([\text{NTf}_2]^-)$ -based ILs, combined with the following cations: 1,3-dimethylimidazolium, $[\text{C}_1\text{C}_1\text{im}]^+$; 1-propyl-3-methylimidazolium, $[\text{C}_3\text{C}_1\text{im}]^+$; 1-pentyl-3-methylimidazolium, $[\text{C}_5\text{C}_1\text{im}]^+$; 1-hexyl-3-methylimidazolium $[\text{C}_6\text{C}_1\text{im}]^+$; ethylimidazolium, $[\text{C}_2\text{im}]^+$; 1,3-diethylimidazolium, $[\text{C}_2\text{C}_2\text{im}]^+$; 1-ethyl-3-methylimidazolium, $[\text{C}_2\text{C}_3\text{im}]^+$; and 1,3-dipropylimidazolium, $[\text{C}_3\text{C}_3\text{im}]^+$. All ILs were supplied from Iolitec. Before the equilibrium experiments, individual samples of all ILs were kept at constant agitation under vacuum and at moderate temperature (323 K), for a minimum of 24 hours, in order to reduce the volatile impurities content to negligible values. After this purification step, the purity of each IL was further checked by ^1H , ^{13}C and ^{19}F NMR spectra and found to be > 99 wt % for all samples. The AC was supplied by Merck (CAS Number: 7440-44-0) and the water used was double distilled.

2.2.2 Experimental procedure

The adsorption tests were carried out in a closed bottle, containing 50 mL of an aqueous solution of each IL at different concentrations and 12.5 mg of AC. All experiments were performed at 308.0 K (± 0.1 K). This temperature was chosen to allow the comparison between the experimental adsorption isotherms gathered in this work with those already published in literature [31]. The samples were kept under continuous shaking in an orbital shaker at 200 rpm, and for at least 5 days, to achieve the complete phase equilibrium. The equilibrium concentration of IL in the liquid phase was measured using a SHIMADZU UV-1700, Pharma-Spec spectrometer at a wavelength of 211 nm, since this wavelength was found to be the maximum length for the imidazolium cation core. The equilibrium concentration in the solid phase ($q_e / \text{mmol} \cdot \text{g}^{-1}$) was calculated using **Equation 1**,

$$q_e = \frac{(C_i - C_e)}{m_{ads}} \times V \quad \text{Eq. 1}$$

where C_i ($\text{mmol} \cdot \text{L}^{-1}$) is the initial concentration of IL in the aqueous solution, C_e ($\text{mmol} \cdot \text{L}^{-1}$) is the equilibrium concentration of IL in the liquid phase, m_{ads} (g) is the mass of adsorbent used in each sample and V (L) is the total volume of the solution in equilibrium.

For the AC characterization a MICROMERITICS Gemini 280 was used, and the BET (A_{BET}) and external (A_{ext}) areas were calculated with the BET equation and the t-method, respectively, as described in [38]. The micropore volume (V_{micro}) was calculated with the Broekhoff-De-Boer equation described by Lecloux *et al.* [39].

The isotherms were obtained fitting the experimental data with two common models: Freundlich (**Equation 2**) and Langmuir (**Equation 3**). These two models are usually applied to both physical and chemical adsorptions [35].

$$q_e = K_f \times C_e^n \quad \text{Eq. 2}$$

$$q_e = \frac{q_{max} \times L \times C_e}{1 + L \times C_e} \quad \text{Eq. 3}$$

where K_f and n are the empirical coefficients of the Freundlich equation, q_{max} ($\text{mmol}\cdot\text{g}^{-1}$) is the maximum capacity of the adsorbent, and L is the ratio of the adsorption-desorption constants.

In order to allow the comparisons regarding the capacity of AC to adsorb each IL, the apparent distribution coefficient was calculated using **Equation 4**.

$$K_d = \frac{q_e}{C_e} \times 1000 \quad \text{Eq. 4}$$

where K_d is the apparent distribution coefficient ($\text{L}\cdot\text{kg}^{-1}$) and q_e ($\text{mmol}\cdot\text{g}^{-1}$) is the value observed when C_e is equal to $1.5 \text{ mmol}\cdot\text{L}^{-1}$ (the factor 1000 is in the equation to achieve desirable units for K_d).

2.3 Results and Discussion

To confirm the existence of pores in the GAC, a sample was taken to perform the characterization of the adsorbent. The characterization of the GAC is presented in **Table 3**.

Table 3 - Characterization of the GAC used in this work.

Adsorbent	$A_{\text{BET}} / (\text{m}^2\cdot\text{g}^{-1})$	$A_{\text{ext}} / (\text{m}^2\cdot\text{g}^{-1})$	$V_{\text{micro}} / (\text{cm}^3\cdot\text{g}^{-1})$
GAC	915.1	109.7	0.363

The values obtained are in good agreement with literature data [9].

The adsorption isotherms of all the $[\text{NTf}_2]$ -based ILs investigated, at 308.0 K, are presented in **Figure 5**.

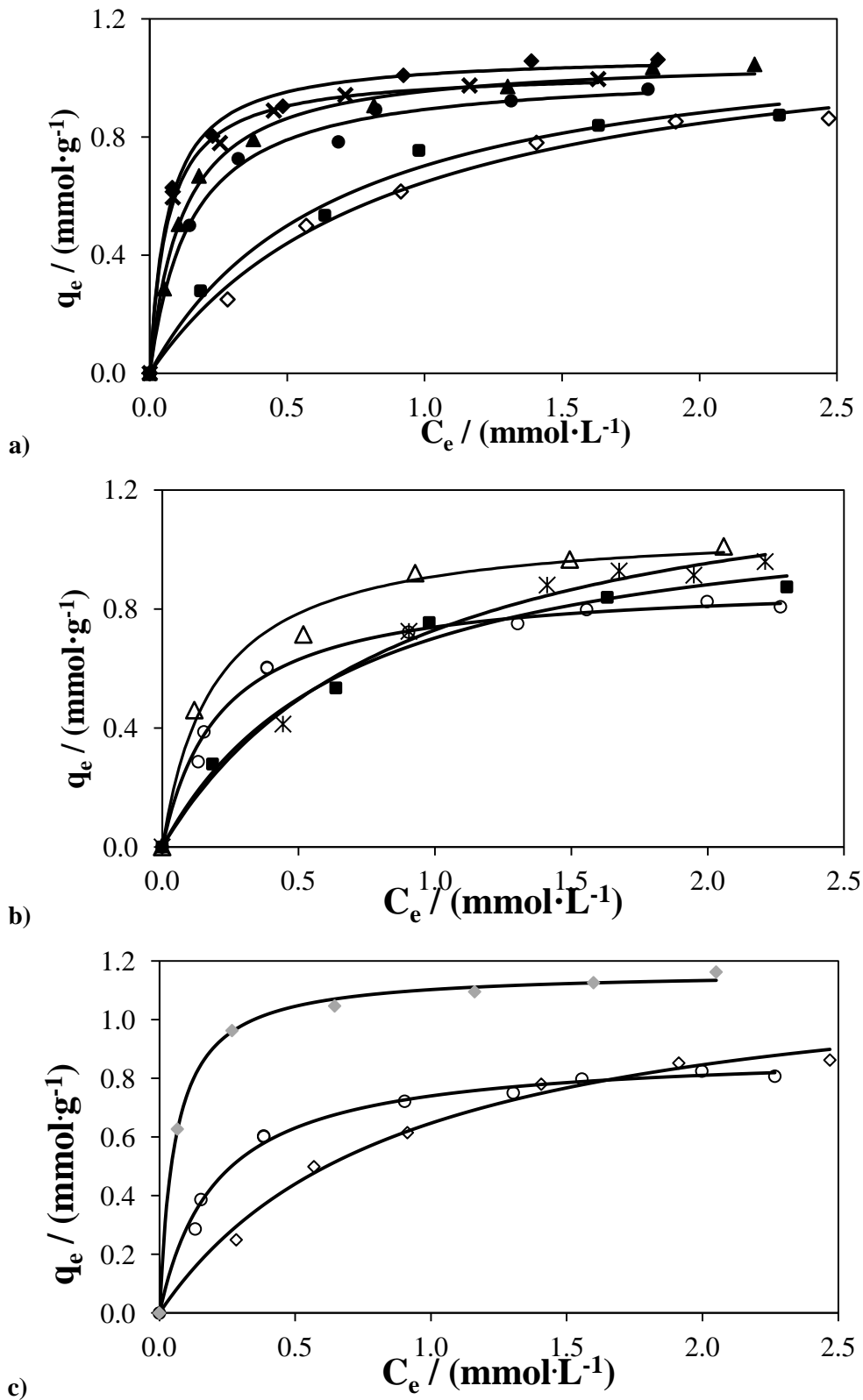


Figure 5 - Adsorption isotherms for comparing the increase of the alkyl side chain length in ILs at 308.0 K: a), (\diamond) $[\text{C}_1\text{C}_1\text{im}][\text{NTf}_2]$, (\blacksquare) $[\text{C}_2\text{C}_1\text{im}][\text{NTf}_2]$, (\bullet) $[\text{C}_3\text{C}_1\text{im}][\text{NTf}_2]$, (\blacktriangle) $[\text{C}_4\text{C}_1\text{im}][\text{NTf}_2]$, (\blacklozenge) $[\text{C}_5\text{C}_1\text{im}][\text{NTf}_2]$, (\times) $[\text{C}_6\text{C}_1\text{im}][\text{NTf}_2]$; b) ($*$) $[\text{C}_2\text{im}][\text{NTf}_2]$, (\circ) $[\text{C}_2\text{C}_2\text{im}][\text{NTf}_2]$, (\triangle) $[\text{C}_2\text{C}_3\text{im}][\text{NTf}_2]$; c), (\blacklozenge) $[\text{C}_3\text{C}_3\text{im}][\text{NTf}_2]$, $[\text{C}_2\text{C}_2\text{im}][\text{NTf}_2]$, (\diamond) $[\text{C}_1\text{C}_1\text{im}][\text{NTf}_2]$.

The experimental data were also fitted with the Freundlich and Langmuir models described in **Equations 2 and 3**. The parameters and correlation coefficients (R^2) are presented in **Appendix A**, namely **Table A1** and **Table A2** for the Freundlich and Langmuir models. The model that better describes the experimental data is the Langmuir model with a R^2 higher than 0.98.

From **Figure 5**, it is evident that the adsorption of the IL increases with the alkyl side chain length of the imidazolium ring. This trend can be explained by the increasing of the hydrophobicity of the IL with the increase in the aliphatic chain which favours the IL adsorption onto the solid phase. This tendency is observed in **Figure 5** for all the IL isomers. The maximum capacity adsorbed is verified for $[\text{C}_5\text{C}_1\text{im}][\text{NTf}_2]$ with a value of $1.05 \text{ mmol}\cdot\text{g}^{-1}$. Concerning the isomers, the maximum capacity was observed for $[\text{C}_3\text{C}_3\text{im}][\text{NTf}_2]$ and the value is $1.16 \text{ mmol}\cdot\text{g}^{-1}$. It is also possible to observe that for ILs with a smaller side chain length ($n < 3$ in $[\text{C}_n\text{C}_1\text{im}]^+$) and for $[\text{C}_2\text{im}]^+$ the isotherms studied did not reach the equilibrium plateau.

In **Table 4** are presented the apparent distribution capacity of the ILs studied. The $[\text{C}_8\text{C}_1\text{im}][\text{NTf}_2]$ and $[\text{C}_{12}\text{C}_1\text{im}][\text{NTf}_2]$ values were taken from literature [31] and are included here for comparison purposes.

Table 4 - K_d values of the ILs studied.

IL	$K_d / (\text{L}\cdot\text{kg}^{-1})$
$[\text{C}_2\text{im}][\text{NTf}_2]$	577.6
$[\text{C}_1\text{C}_1\text{im}][\text{NTf}_2]$	512.6
$[\text{C}_2\text{C}_1\text{im}][\text{NTf}_2]$	540.8
$[\text{C}_2\text{C}_2\text{im}][\text{NTf}_2]$	545.9
$[\text{C}_3\text{C}_1\text{im}][\text{NTf}_2]$	621.9
$[\text{C}_2\text{C}_3\text{im}][\text{NTf}_2]$	640.6
$[\text{C}_4\text{C}_1\text{im}][\text{NTf}_2]$	660.2
$[\text{C}_3\text{C}_3\text{im}][\text{NTf}_2]$	748.0
$[\text{C}_5\text{C}_1\text{im}][\text{NTf}_2]$	689.1
$[\text{C}_6\text{C}_1\text{im}][\text{NTf}_2]$	653.7
$[\text{C}_8\text{C}_1\text{im}][\text{NTf}_2]$	601.1 [31]
$[\text{C}_{12}\text{C}_1\text{im}][\text{NTf}_2]$	546.3 [31]

The values observed for K_d range between 513 and 748 L·kg⁻¹. The maximum capacity adsorbed on AC, for the asymmetric ILs, is gathered with [C₅C₁im][NTf₂] and its K_d value is 698.5 L·kg⁻¹. For ILs with longer alkyl side chains ($n > 5$ in [C_{*n*}C₁im]⁺) the adsorption capacity decreases. In these examples the ionic liquid cation becomes too large and their diffusion in the pores becomes more difficult. The adsorption capacity in terms of K_d for the [C_{*n*}C_{*n*}im]-based series is lower when compared with their isomers. Nevertheless, these differences tend to disappear as the alkyl chain increases. In fact, it will eventually reverse as can be seen in the comparison between [C₃C₃im][NTf₂] and [C₅C₁im][NTf₂].

Figure 6 compares the adsorption of the IL isomers with the same total number of carbons in the alkyl side chains of the cation.

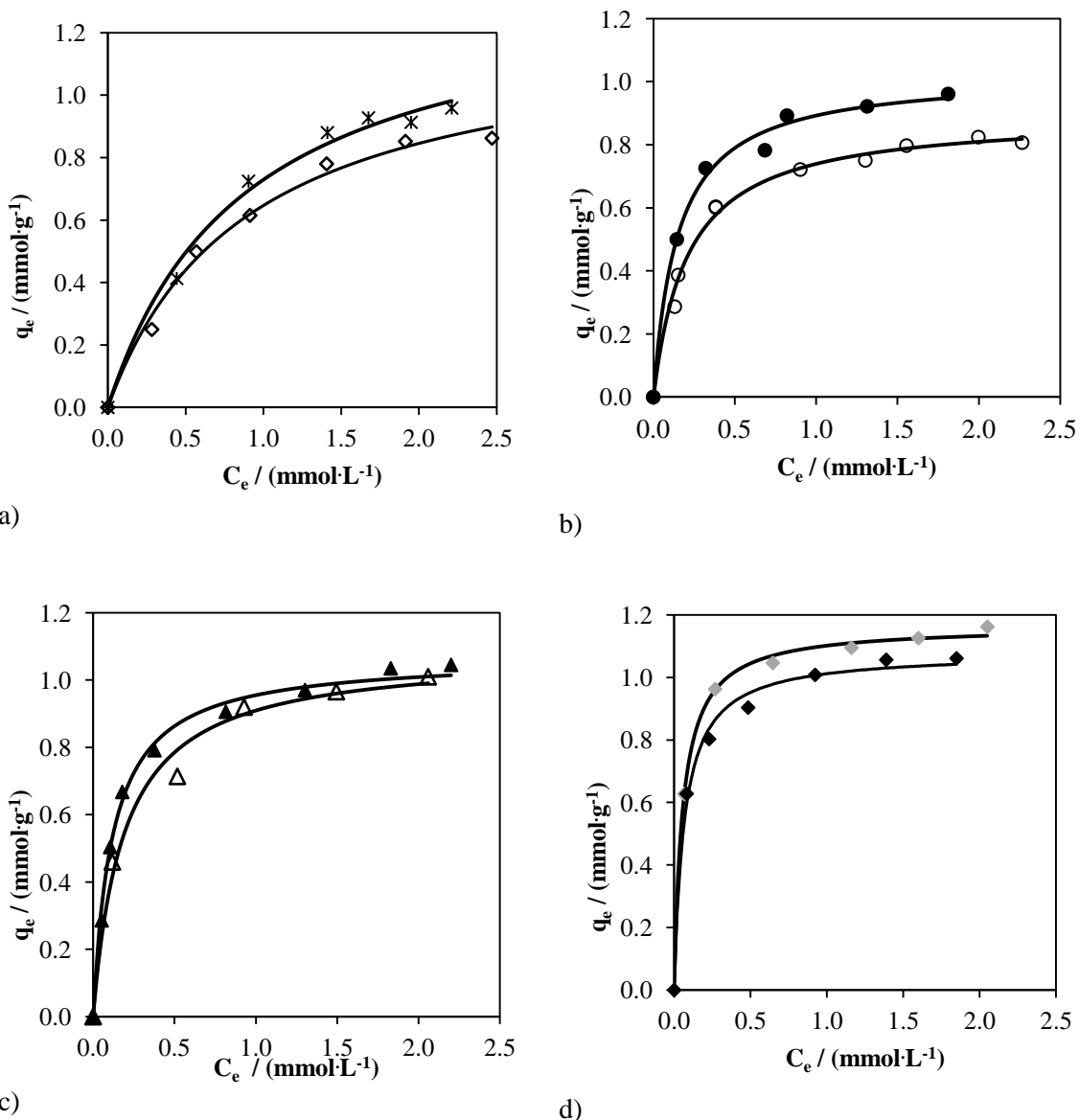


Figure 6 - Adsorption isotherms for comparing the isomeric ILs at 308.0 K: a) (*), [C₂im][NTf₂], (◇) [C₁C₁im][NTf₂]; b), (●) [C₃C₁im][NTf₂], (○) [C₂C₂im][NTf₂]; c) (▲) [C₄C₁im][NTf₂], (△) [C₂C₃im][NTf₂], d); (◆) [C₅C₁im][NTf₂], (◇) [C₃C₃im][NTf₂].

Figure 6 shows that for the *N,N*-dialkylimidazolium-based ILs the adsorption capacity is lower than that observed for the 1-alkyl-3-methylimidazolium-based ILs. After five carbons (total number of carbons in the aliphatic chains of the imidazolium cation) the trend changes: [C₅C₁im][NTf₂] has lower adsorption capacity than its isomer [C₃C₃im][NTf₂]. This result is in conformation with their K_d values, 689.1 and 748.0 L·kg⁻¹, respectively.

2.4 Conclusions

In this work it was evaluated the capacity of activated charcoal for removing hydrophobic ILs from aqueous effluents. To this end, several [NTf₂]-based ILs were investigated and the influence of the cation side alkyl chain length and isomerism of the cation were analysed. From the gathered results, it can be concluded that the adsorption of the IL increases with the alkyl side chain length of the imidazolium cation for both series investigated. For longer alkyl side chains the adsorptions starts to decrease. The [C_nC_nim]-based series has a lower adsorption capacity compared to their isomers in the [C_nC₁im]-based series. However, when the total number of carbons exceeds 5 carbons the trend inverts. The maximum adsorption capacity observed was for [C₃C₃im][NTf₂] (1.16 g·mol⁻¹) with a *K_d* value of 748.0 L·kg⁻¹.

For all of the ILs studied both the Langmuir and the Freundlich model were used to fit the experimental data. For all systems investigated, the Langmuir model better describes the experimental data and is in close agreement with literature [9].

3 Recovery of ILs using Aqueous Biphasic Systems

3.1 Introduction

Aqueous biphasic systems (ABS) are formed when two mutually incompatible aqueous solutions composed of polymer/polymer, polymer/salt or salt/salt are mixed. Above a given concentration of those components, spontaneous phase separation takes place [41, 42].

ABS have been extensively and particularly exploited as liquid-liquid extraction techniques for the recovery of biological products, such as proteins, enzymes and amino acids [43, 44]. The advantages of using ABS over conventional techniques, which use volatile and organic solvents, relies on their short processing time, low energy consumption, little emulsion formation, biocompatible environment, economical and efficient downstream, and their easy scale-up [45-47].

Typical ABS are composed of polymers and conventional salts [41, 42]. Nevertheless, Rogers and co-workers [48] showed that hydrophilic ILs can also form ABS in the presence of inorganic salts. Not all the inorganic salts are capable of forming ABS with ILs [47], and Rogers et al. [48] suggested that salts containing “kosmotropic” ions, such as HPO_4^{2-} , SO_4^{2-} , OH^- , PO_4^{3-} or CO_3^{2-} can easily induce the formation of IL-based ABS formation, whereas “chaotropic” ions, such as Cl^- , NH_4^+ , K^+ and H_2PO_4^- do not lead to liquid-liquid demixing. This rank of ions is usually comprised in the salting-out and salting-in phenomena and Hofmeister series [49]. Besides the influence of the salt in the formation of ABS, ILs also have a strong impact towards their ABS behaviour. Some studies have addressed this effect [50, 51].

Rogers and co-workers [48] stated that IL-based ABS can be utilized to recycle or concentrate hydrophilic ILs from aqueous solutions, *i.e.*, the addition of an inorganic salt inevitably leads to an IL-rich phase and a salt-rich phase. After this statement [48], additional studies have appeared in literature. Zhang et al. [52] reported that $[\text{aC}_1\text{im}]\text{Cl}$ could be recovered from aqueous solutions using ABS. The recovery efficiency was 96.8 % using 47 wt % of K_2HPO_4 [52]. In addition, Bo et al. [53, 54] reported some recovery efficiencies of ILs from aqueous media by the addition of common sugars. The highest recovery was observed with $[\text{C}_4\text{C}_1\text{im}][\text{BF}_4]$ with a value of 74 %.

Taking into account the possibility of using ABS to recover ILs from aqueous media, in this work, several ILs were tested combined with sodium carbonate (Na_2CO_3).

The selection of Na_2CO_3 as phase promoter agent is supported by its good salting-out ability [46] and by the promising results previously reported by Li et al. [41].

3.2 Experimental Section

3.2.1 Materials

The ionic liquids studied in the formation of ABS were 1-butyl-3-methylimidazolium trifluoromethanesulfonate (triflate), $[\text{C}_4\text{C}_1\text{im}][\text{CF}_3\text{SO}_3]$, 1-butyl-3-methylimidazolium thiocyanate, $[\text{C}_4\text{C}_1\text{im}][\text{SCN}]$, 1-butyl-3-methylimidazolium methanesulfonate, $[\text{C}_4\text{C}_1\text{im}][\text{CH}_3\text{SO}_3]$, 1-butyl-3-methylimidazolium ethylsulfate, $[\text{C}_4\text{C}_1\text{im}][\text{C}_2\text{H}_5\text{SO}_4]$, 1-butyl-3-methylimidazolium methylsulfate, $[\text{C}_4\text{C}_1\text{im}][\text{CH}_3\text{SO}_4]$, 1-butyl-3-methylimidazolium tosylate, $[\text{C}_4\text{C}_1\text{im}][\text{Tos}]$, 1-butyl-3-methylimidazolium bromide, $[\text{C}_4\text{C}_1\text{im}]\text{Br}$, 1-butyl-3-methylimidazolium dicyanamide, $[\text{C}_4\text{C}_1\text{im}][\text{N}(\text{CN})_2]$, 1-butyl-3-methylimidazolium dimethylphosphate, $[\text{C}_4\text{C}_1\text{im}][\text{DMP}]$, 1-butyl-3-methylimidazolium chloride, $[\text{C}_4\text{C}_1\text{im}]\text{Cl}$, 1-ethyl-3-methylimidazolium chloride, $[\text{C}_2\text{C}_1\text{im}]\text{Cl}$, 1-hexyl-3-methylimidazolium chloride, $[\text{C}_6\text{C}_1\text{im}]\text{Cl}$, 1-allyl-3-methylimidazolium chloride, $[\text{aC}_1\text{im}]\text{Cl}$, 1-butyl-1-methylpyrrolidinium chloride, $[\text{C}_4\text{C}_1\text{pyr}]\text{Cl}$, 1-butyl-3-methylpiperidinium chloride, $[\text{C}_4\text{C}_1\text{pip}]\text{Cl}$, 1-butylpyridinium chloride, $[\text{C}_4\text{py}]\text{Cl}$, 1-butyl-2-methylpyridinium chloride, $[\text{C}_4\text{-2-C}_1\text{py}]\text{Cl}$, 1-butyl-3-methylpyridinium chloride, $[\text{C}_4\text{-3-C}_1\text{py}]\text{Cl}$, 1-butyl-4-methylpyridinium chloride, $[\text{C}_4\text{-4-C}_1\text{py}]\text{Cl}$, tetrabutylammonium chloride, $[\text{N}_{4444}]\text{Cl}$, and tetrabutylphosphonium chloride, $[\text{P}_{4444}]\text{Cl}$. All imidazolium-, pyridinium-, and pyrrolidinium-based ionic liquids were supplied from Iolitec. The tetrabutylphosphonium chloride was kindly supplied by Cytec Industries Inc. and the tetrabutylammonium chloride was from Aldrich. Individual samples of ILs were kept at constant agitation under vacuum and at moderate temperature (323 K), for a minimum of 24 hours in order to reduce the volatile impurities content to negligible values. After this purification step, the purity of each IL was further checked by ^1H , ^{13}C and ^{19}F NMR (whenever applicable) spectra and found to be > 98 wt % for all samples. Na_2CO_3 was from PROLABO (purity > 99.9 wt %). and the water used was double distilled.

3.2.2 Experimental procedure

The solubility curves of the systems composed of IL, water, and sodium carbonate (Na_2CO_3) were determined using the visual determination of the cloud point by the titration method at 298 K (± 1 K) and at atmospheric pressure.

Aqueous solutions of Na_2CO_3 with mass fractions of approximately 20 wt %, and aqueous solutions of each IL with mass fraction of approximately 60 wt % were prepared and used for the determination of the corresponding solubility curves. Repetitive drop-wise addition of the aqueous salt solution to each IL aqueous solution was carried out until the detection of a cloudy solution (the biphasic region), followed by the drop-wise addition of water until the formation of a clear and limpid solution (the monophasic region). To complete the phase diagrams the opposite addition of the IL, in this case with mass fraction of approximately 80 wt % to the aqueous solution of the salt was also carried out. Drop-wise additions were carried out under constant stirring. The ternary systems compositions were determined by weight quantification of all components within $\pm 10^{-4}$ g.

The experimental binodal curves were fitted by least-squares regression according to **Equation 5**,

$$[IL] = A \times e^{(B \times [Salt]^{0.5} - (C \times [Salt]^3))} \quad \text{Eq. 5}$$

where [IL] and [Salt] are the ionic liquid and the inorganic salt weight fraction percentages, respectively, and A , B and C are fitted constants obtained by the regression of the experimental data. For the determination of each tie-line (TL), a ternary mixture composed of Na_2CO_3 / H_2O / IL at the biphasic region was gravimetrically prepared within $\pm 10^{-4}$ g, vigorously stirred, and left to equilibrate for at least 12 hours at 298 K (± 1 K), to achieve a complete separation of the coexisting aqueous phases. The phases were further separated and individually weighed within $\pm 10^{-4}$ g. Each TL was determined through the relationship between the weight of the IL-rich phase and the overall weight of the mixture by the lever-arm rule and for which the following system of four equations (**Equations 6 to 9**) and four unknown values ($[\text{IL}]_{\text{T}}$, $[\text{IL}]_{\text{B}}$, $[\text{Salt}]_{\text{T}}$ and $[\text{Salt}]_{\text{B}}$) was solved,

$$[IL]_{\text{T}} = A \times e^{(B \times [Salt]_{\text{T}}^{0.5} - (C \times [Salt]_{\text{T}}^3))} \quad \text{Eq. 6}$$

$$[IL]_B = A \times e^{(B \times [Salt]_B^{0.5} - (C \times [Salt]_B^3))} \quad \text{Eq. 7}$$

$$[IL]_T = \frac{[IL]_M}{\alpha} - \frac{1-\alpha}{\alpha} \times [IL]_B \quad \text{Eq. 8}$$

$$[Salt]_T = \frac{[Salt]_M}{\alpha} - \frac{1-\alpha}{\alpha} \times [Salt]_B \quad \text{Eq. 9}$$

“T”, “B”, and “M” designate the top phase, the bottom phase and the mixture, respectively, and α is the ratio between the mass of the top phase and the total mass of the mixture. The system solution results in the mass fraction percentage of the IL and inorganic salt in the top and bottom phases, and thus represents the TLs of each system.

In order to evaluate the recovery efficiencies of ILs from aqueous solutions, **Equation 10** was applied to all the experimentally measured TLs,

$$\% R = \frac{[IL]_T \times m_T}{[IL]_T \times m_T + [IL]_B \times m_B} \quad \text{Eq. 10}$$

where “T” and “B” symbolize, respectively, the ionic-liquid- (top) and salt-rich (bottom) phases, [Salt] and [IL] are the weight fraction percentage of inorganic salt and ionic liquid, and m is the weight of each phase.

3.3 Results and Discussion

All phase diagrams or binodal curves are presented in terms of weight fraction for comparison purposes and to address on the weight of salt/IL needed to have the formation of two phases. The experimental data were fitted by **Equation 5**. All the fittings present high correlation coefficients, R^2 , higher than 0.99. **Appendix B (Tables B26 and B27)** presents the fitting parameters obtained and respective correlation coefficients for each system.

The experimental results obtained for the ternary mixtures of H₂O, Na₂CO₃ and [C₄C₁im]-based ILs are presented in **Figure 7**. This figure allows the comparison on the

anion effect towards the formation of ABS. In addition, **Figure 8** represents the effect of the cation core on ABS formation.

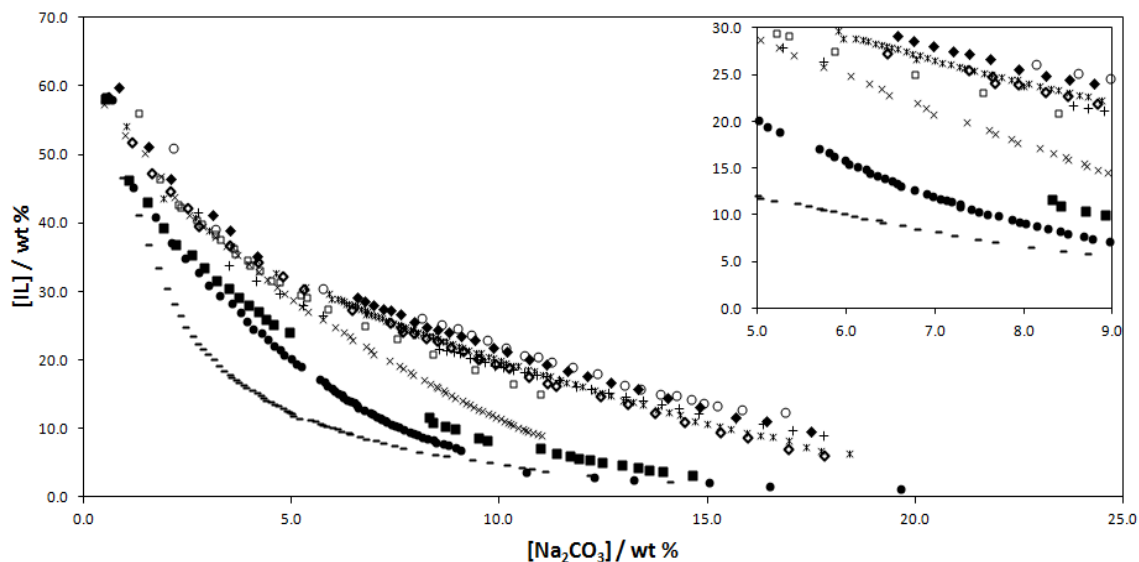


Figure 7 - Binodal curves for the $[C_4C_1im]$ -based ILs at 298 K: (\times) $[C_4C_1im][Tos]$; (—) $[C_4C_1im][CF_3SO_3]$; (\diamond) $[C_4C_1im][CH_3SO_4]$; (\circ) $[C_4C_1im][DMP]$; (\square) $[C_4C_1im][C_2H_5SO_4]$; (\bullet) $[C_4C_1im][SCN]$; (\blacksquare) $[C_4C_1im][N(CN)_2]$; (\blacklozenge) $[C_4C_1im][CH_3SO_3]$; ($+$) $[C_4C_1im]Cl$; ($*$) $[C_4C_1im]Br$.

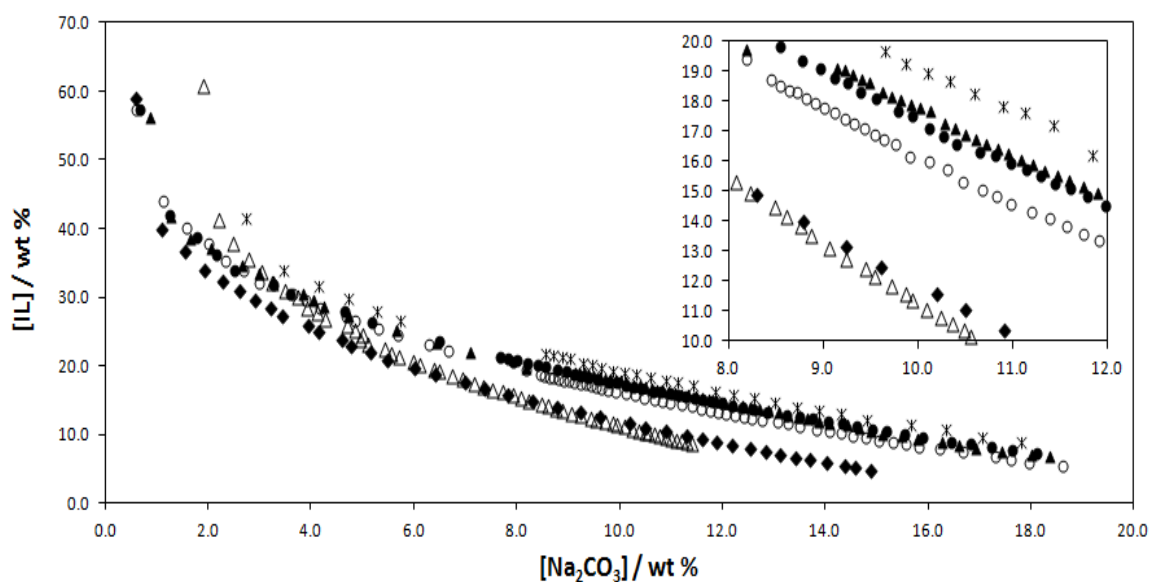


Figure 8 - Binodal curves for the Cl-based ILs at 298 K: ($*$) $[C_4C_1im]Cl$; (\circ) $[C_4C_1pip]Cl$; (\blacktriangle) $[C_4-3-C_1pyr]Cl$; (\bullet) $[C_4C_1pyr]Cl$; (\blacklozenge) $[N_{4444}]Cl$; (\triangle) $[P_{4444}]Cl$.

The biphasic region is above the binodal curve and the monophasic region is under the binodal curve. The larger the biphasic region is, the higher the ability of each IL to undergo ABS formation [53]. From **Figure 7**, the ability of the $[C_4C_1im]$ -based ILs to form ABS follows the order: $[CF_3SO_3]^- > [SCN]^- > [N(CN)_2]^- > [Tos]^- > [C_2H_5SO_4]^- > [CH_3SO_4]^- > Cl^- > Br^- > [CH_3SO_3]^- > [DMP]^-$. The results show a strong dependency of the anion for the ABS formation. In general, low amounts of Na_2CO_3 are able to induce the separation of an IL-rich phase.

From **Figure 8** it is possible to see that the influence of the cation on the ABS formation is much weaker than that of the anion. The ability of the chloride-based ILs to form ABS follows the trend: $[P_{4444}]^+ \approx [N_{4444}]^+ > [C_4C_1pip]^+ \approx [C_4C_1pyr]^+ \approx [C_4-3-C_1py]^+ \approx [C_4C_1im]^+$. The phosphonium- and ammonium-based ILs with four butyl chains are more easily separated from aqueous media when compared to cyclic nitrogen-based ILs.

The influence of the increase of the alkyl side chain length of the cation is shown in **Figure 9**. **Figure 10** shows the positional isomerism influence making use of several pyridinium-based cations with a methyl group at different positions.

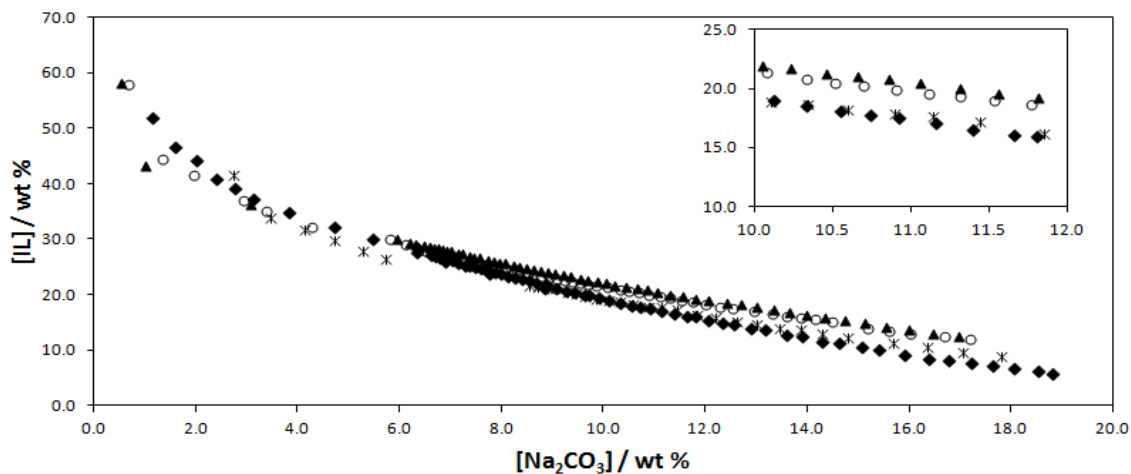


Figure 9 - Binodal curves for imidazolium-chloride-based ILs at 298 K: (*) $[C_4C_1im]Cl$; (\blacktriangle) $[C_2C_1im]Cl$; (\blacklozenge) $[C_6C_1im]Cl$; (\circ) $[aC_1im]Cl$.

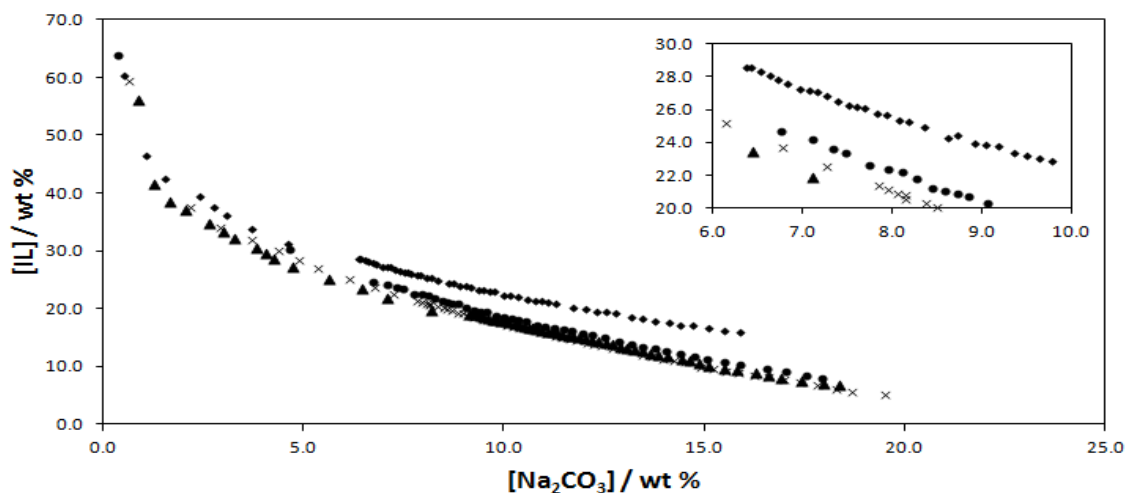


Figure 10 - Binodal curves for pyridinium-based isomeric ILs at 298 K: (▲) [C₄-3-C₁py]Cl; (×) [C₄-4-C₁py]Cl; (●) [C₄-2-C₁py]Cl; (◆) [C₄py]Cl.

Figure 9 reveals that with the increase on the alkyl side chain of the imidazolium cation, the ability to form ABS also increases. With the increase in the alkyl side chain there is an increase in the hydrophobicity of the IL and thus a lower affinity for water.

From **Figure 10** it can be seen that the position of the methyl group at the pyridinium cation has no major influence towards the ABS formation ability. However, the removal of a methyl group in these ILs, to form [C₄py]Cl, decreases the ability of the IL to phase separate.

Figure 11 presents the recovery efficiency (% *R*) (**Equation 10**) of all ILs studied making use of the addition of the Na₂CO₃ salt. The compositions of each phase and each TL as well as the mass of the bottom and top phases are presented in **Appendix B, Tables B28 and B29**, respectively.

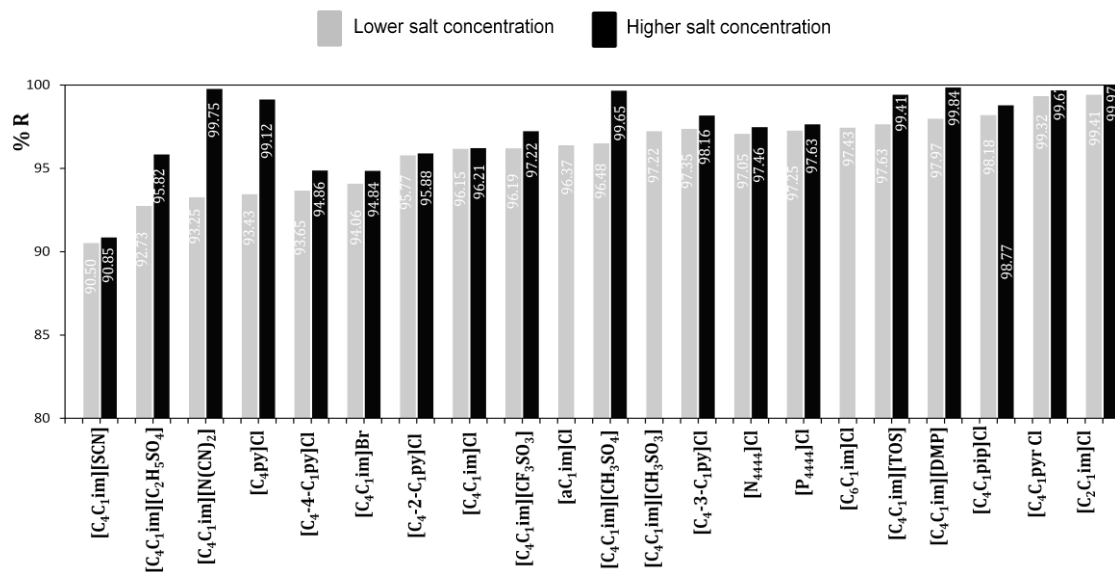


Figure 11 - Percentage recovery efficiency (% *R*) of ILs.

The salt concentrations used to promote the recovery of the IL for the IL-rich phase range between 3.4 and 14.0 wt %. The IL contents range between 20.0 and 34.0 wt %. From Figure 11, it is possible to conclude that the recovery efficiencies obtained are always higher than 90 % for all the ILs investigated. The maximum recovery efficiency achieved was 99.97 % for [C₂C₁im]Cl. Concerning the anions influence in the [C₄C₁im]-based ILs, the higher recovery efficiency was observed for [C₄C₁im][N(CN)₂] with a 99.75 % of recovery. Regarding the cation effect, the recovery efficiencies decrease in the order: pyrrolidinium > piperidinium > pyridinium > imidazolium > phosphonium ≈ ammonium. The ILs composed of the two non-cyclic cations present similar recovery efficiencies, 97.05 % and 97.25 %, for [N₄₄₄₄]Cl and [P₄₄₄₄]Cl, respectively. In this work it was possible to achieve a recovery efficiency of 96.37 % for [aC₁im]Cl which is indeed close to that observed by Zang [52] (96.8 % with K₂HPO₄). Nevertheless, it should be remarked that in this work a considerably lower amount of salt was used to obtain high recovery efficiencies – a direct effect of the strong salting-out potential of the salt employed.

Figure 12 depicts a schematic process to apply on effluents contaminated with large amounts of hydrophilic ILs. The main process consists in the use of ABS in which two different streams are generated: one IL-rich phase on the top and a salt-rich phase on the bottom. The concentrated inorganic salt solution could be recycled and enter again into the main process.

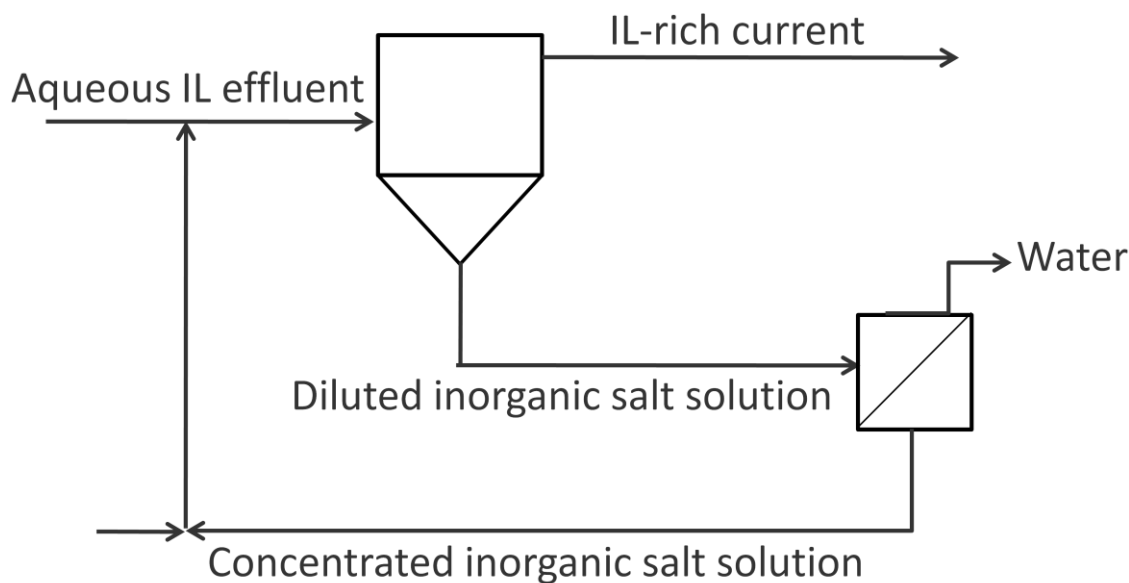


Figure 12 - Scheme for the water treatment process making use of ABS.

3.4 Conclusions

In this section it was evaluated the capacity of Na_2CO_3 to induce the formation of ABS and the possibility of removing and recovering ILs from aqueous effluents. A large range of ILs was evaluated and the effect of the anion nature, cation core, alkyl side chain length, and isomerism of the cation of the IL were addressed towards their ability to form ABS and by their recovery efficiencies. The aptitude of $[\text{C}_4\text{C}_1\text{im}]$ -based ILs to form ABS decreases in the order: $[\text{CF}_3\text{SO}_3]^- > [\text{SCN}]^- > [\text{N}(\text{CN})_2]^- > [\text{Tos}]^- > [\text{C}_2\text{H}_5\text{SO}_4]^- > [\text{CH}_3\text{SO}_4]^- > \text{Cl}^- > \text{Br}^- > [\text{CH}_3\text{SO}_3]^- > [\text{DMP}]^-$. The effect of the anion is more relevant than the influence of the cation where the following rank was observed: $[\text{C}_4\text{C}_1\text{im}]^+ \approx [\text{C}_4\text{-3-C}_1\text{py}]^+ \approx [\text{C}_4\text{C}_1\text{pyr}]^+ \approx [\text{C}_4\text{C}_1\text{pip}]^+ < [\text{N}_{4444}]^+ \approx [\text{P}_{4444}]^+$. In addition, an increase in the cation side alkyl chain length leads to an increasing ability to form ABS whereas the positional isomerism of the cation has no major effect.

Finally, the recovery efficiencies obtained for all the ILs studied were higher than 90 % justifying the use of this type of approach for the treatment of aqueous effluents contaminated with large amounts of ILs.

4 Final Remarks

4.1 Future Work

Taking into account the gathered results obtained for the adsorption, the next step should involve desorption tests to recover the IL adsorbed and to reuse the AC. Furthermore, additional experiments on the effect of temperature in the adsorption isotherms should be carried out to ascertain on its effect. Also, other hydrophobic ILs should be investigated.

Novel sorbents, like zeolites, should also be tested regarding their ability to adsorb ILs.

Regarding the ABS used for recovering ILs that are present in higher concentrations, additional comparisons between the recovery efficiencies obtained with Na_2CO_3 and other salts should be performed. In this context, it will be important to study other strong salting-out salts and the possible formation of IL-based ABS.

A desalinization method should also be proposed in order to remove the Na_2CO_3 that is still in the IL-rich phase (even if in small amounts) to allow the recovery of pure ILs. For example, membrane processes and HCl addition should be investigated in the future.

5 References

5.1 References:

- [1] P. Walden, "Über die Molekulargröße und elektrische Leitfähigkeit einiger geschmolzenen Salze", *Bulletin de l'Académie Impériale des Sciences de St.-Petersbourg* vol. 8, pp. 405-422, 1914.
- [2] N. V. Plechkova and K. R. Seddon, "Applications of ionic liquids in the chemical industry", *Chemical Society Reviews*, vol. 37, pp. 123-150, 2008.
- [3] M. J. Earle and K. R. Seddon, "Ionic Liquids: Green Solvents for the Future", in *Clean Solvents*. vol. 819, ed: American Chemical Society, 2002, pp. 10-25.
- [4] B. Kirchner, *Topics in Current Chemistry* vol. 290: Springer, 2009.
- [5] K. Marsh, A. Deev, A. Wu, E. Tran, and A. Klamt, "Room temperature ionic liquids as replacements for conventional solvents – A review", *Korean Journal of Chemical Engineering*, vol. 19, pp. 357-362, 2002.
- [6] T. P. Thuy Pham, C.-W. Cho, and Y.-S. Yun, "Environmental fate and toxicity of ionic liquids: A review", *Water Research*, vol. 44, pp. 352-372, 2010.
- [7] K. R. Seddon, "Ionic Liquids for Clean Technology", *Journal of Chemical Technology & Biotechnology*, vol. 68, pp. 351-356, 1997.
- [8] M. Koel, *Ionic liquids in Chemical Analysis*: CRC Press, 2009.
- [9] J. Palomar, J. Lemus, M. A. Gilarranz, and J. J. Rodriguez, "Adsorption of ionic liquids from aqueous effluents by activated carbon", *Carbon*, vol. 47, pp. 1846-1856, 2009.
- [10] J. F. Wishart, "Energy applications of ionic liquids", *Energy & Environmental Science*, vol. 2, 2009.
- [11] R. L. Gardas and J. A. P. Coutinho, "Group contribution methods for the prediction of thermophysical and transport properties of ionic liquids", *AIChE Journal*, vol. 55, pp. 1274-1290, 2009.

- [12] N. Gathergood, M. T. Garcia, and P. J. Scammells, "Biodegradable ionic liquids: Part I. Concept, preliminary targets and evaluation", *Green Chemistry*, vol. 6, 2004.
- [13] J. Kärkkäinen, "Preparation and characterization of some ionic liquids and their use in the dimerization reaction of 2 - methylpropene", Master Thesis, Department of Chemistry, University of Oulu, Finland, 2007.
- [14] L. Moller, D. Schuetzle, and H. Autrup, "Future research needs associated with the assessment of potential human health risks from exposure to toxic ambient air pollutants", *Environmental health perspectives*, vol. 102 Suppl 4, pp. 193-210, 1994.
- [15] M. A. Lillo-Ródenas, D. Cazorla-Amorós, and A. Linares-Solano, "Behaviour of activated carbons with different pore size distributions and surface oxygen groups for benzene and toluene adsorption at low concentrations", *Carbon*, vol. 43, pp. 1758-1767, 2005.
- [16] M. G. Freire, C. M. S. S. Neves, P. J. Carvalho, R. L. Gardas, A. M. Fernandes, I. M. Marrucho, L. M. N. B. F. Santos, and J. A. P. Coutinho, "Mutual Solubilities of Water and Hydrophobic Ionic Liquids", *The Journal of Physical Chemistry B*, vol. 111, pp. 13082-13089, 2007.
- [17] J. L. Anthony, E. J. Maginn, and J. F. Brennecke, "Solution Thermodynamics of Imidazolium-Based Ionic Liquids and Water", *The Journal of Physical Chemistry B*, vol. 105, pp. 10942-10949, 2001.
- [18] K. R. Seddon, A. Stark, and M. J. Torres, "Influence of chloride, water, and organic solvents on the physical properties of ionic liquids", *Pure Appl. Chem.*, vol. 72, pp. 2275-2287, 2000.
- [19] M. G. Freire, C. M. S. S. Neves, S. P. M. Ventura, M. J. Pratas, I. M. Marrucho, J. Oliveira, J. A. P. Coutinho, and A. M. Fernandes, "Solubility of non-aromatic ionic liquids in water and correlation using a QSPR approach", *Fluid Phase Equilibria*, vol. 294, pp. 234-240, 2010.
- [20] A. M. O'Mahony, D. S. Silvester, L. Aldous, C. Hardacre, and R. G. Compton, "Effect of Water on the Electrochemical Window and Potential Limits of Room-Temperature Ionic Liquids", *Journal of Chemical & Engineering Data*, vol. 53, pp. 2884-2891, 2008.

- [21] C. M. S. S. Neves, "Aqueous Biphasic Systems with Ionic Liquids", Master Degree, Departamento de Química, Universidade de Aveiro, 2009.
- [22] K. M. Docherty and J. C. F. Kulpa, "Toxicity and antimicrobial activity of imidazolium and pyridinium ionic liquids", *Green Chemistry*, vol. 7, 2005.
- [23] J. Ranke, K. Mölter, F. Stock, U. Bottin-Weber, J. Poczobutt, J. Hoffmann, B. Ondruschka, J. Filser, and B. Jastorff, "Biological effects of imidazolium ionic liquids with varying chain lengths in acute *Vibrio fischeri* and WST-1 cell viability assays", *Ecotoxicology and Environmental Safety*, vol. 58, pp. 396-404, 2004.
- [24] F. Stock, J. Hoffmann, J. Ranke, R. Stormann, B. Ondruschka, and B. Jastorff, "Effects of ionic liquids on the acetylcholinesterase - a structure-activity relationship consideration", *Green Chemistry*, vol. 6, 2004.
- [25] J. Arning, S. Stolte, A. Boschen, F. Stock, W.-R. Pitner, U. Welz-Biermann, B. Jastorff, and J. Ranke, "Qualitative and quantitative structure activity relationships for the inhibitory effects of cationic head groups, functionalised side chains and anions of ionic liquids on acetylcholinesterase", *Green Chemistry*, vol. 10, 2008.
- [26] N. Gathergood, P. J. Scammells, and M. T. Garcia, "Biodegradable ionic liquids Part III. The first readily biodegradable ionic liquids", *Green Chemistry*, vol. 8, 2006.
- [27] S. Wang, J. Jacquemin, P. Husson, C. Hardacre, and M. F. Costa Gomes, "Liquid-liquid miscibility and volumetric properties of aqueous solutions of ionic liquids as a function of temperature", *The Journal of Chemical Thermodynamics*, vol. 41, pp. 1206-1214, 2009.
- [28] A. Kokorin, *Ionic Liquids: Theory, Properties, New Approaches*. InTech, 2011.
- [29] P. T. Anastas, P. Wasserscheid, and A. Stark, *Handbook of Green Chemistry, Volume 6: Ionic Liquids*, 2010.
- [30] J. J. Beaulieu, J. L. Tank, and M. Kopacz, "Sorption of imidazolium-based ionic liquids to aquatic sediments", *Chemosphere*, vol. 70, pp. 1320-1328, 2008.

- [31] J. Lemus, J. Palomar, F. Heras, M. A. Gilarranz, and J. J. Rodriguez, "Developing criteria for the recovery of ionic liquids from aqueous phase by adsorption with activated carbon", *Separation and Purification Technology*.
- [32] C. Abrusci, J. Palomar, J. L. Pablos, F. Rodriguez, and F. Catalina, "Efficient biodegradation of common ionic liquids by *Sphingomonas paucimobilis* bacterium", *Green Chemistry*, vol. 13, pp. 709-717, 2011.
- [33] E. M. Siedlecka, M. Gołębiowski, Z. Kaczyński, J. Czupryniak, T. Ossowski, and P. Stepnowski, "Degradation of ionic liquids by Fenton reaction; the effect of anions as counter and background ions", *Applied Catalysis B: Environmental*, vol. 91, pp. 573-579, 2009.
- [34] M. Czerwicka, S. Stolte, A. Müller, E. M. Siedlecka, M. Gołębiowski, J. Kumirska, and P. Stepnowski, "Identification of ionic liquid breakdown products in an advanced oxidation system", *Journal of Hazardous Materials*, vol. 171, pp. 478-483, 2009.
- [35] R. C. Bansal and M. Goyal, *Activated Carbon Adsorption*: CRC Press, 2005.
- [36] F. I. Khan and A. Kr. Ghoshal, "Removal of Volatile Organic Compounds from polluted air", *Journal of Loss Prevention in the Process Industries*, vol. 13, pp. 527-545, 2000.
- [37] M. J. Prauchner and F. Rodríguez-Reinoso, "Chemical versus physical activation of coconut shell: A comparative study", *Microporous and Mesoporous Materials*, vol. 152, pp. 163-171, 2012.
- [38] S. Brunauer, P. H. Emmett, and E. Teller, "*Adsorption of Gases in Multimolecular Layers*", *Journal of the American Chemical Society*, vol. 60, pp. 309-319, 1938.
- [39] A. J. Lecloux, J. Bronckart, F. Noville, and J.-P. Pirard, "*The Generalized Broekhoff-De Boer Method*", in *Studies in Surface Science and Catalysis*. vol. Volume 39, pp. 233-242, 1988.
- [40] J. K. Brennan, T. J. Bandoz, K. T. Thomson, and K. E. Gubbins, "Water in porous carbons", *Colloids and Surfaces A: Physicochemical and Engineering Aspects*, vol. 187-188, pp. 539-568, 2001.

- [41] C. Li, J. Han, Y. Wang, Y. Yan, J. Pan, X. Xu, and Z. Zhang, "Phase Behavior for the Aqueous Two-Phase Systems Containing the Ionic Liquid 1-Butyl-3-methylimidazolium Tetrafluoroborate and Kosmotropic Salts", *Journal of Chemical & Engineering Data*, vol. 55, pp. 1087-1092, 2010/03/11 2009.
- [42] M. Rito-Palomares, "Practical application of aqueous two-phase partition to process development for the recovery of biological products", *Journal of Chromatography B*, vol. 807, pp. 3-11, 2004.
- [43] M. Domínguez-Pérez, L. I. N. Tomé, M. G. Freire, I. M. Marrucho, O. Cabeza, and J. A. P. Coutinho, "(Extraction of biomolecules using) aqueous biphasic systems formed by ionic liquids and aminoacids", *Separation and Purification Technology*, vol. 72, pp. 85-91, 2010.
- [44] J. F. B. Pereira, A. S. Lima, M. G. Freire, and J. A. P. Coutinho, "Ionic liquids as adjuvants for the tailored extraction of biomolecules in aqueous biphasic systems", *Green Chemistry*, vol. 12, pp. 1661-1669, 2010.
- [45] J. A. Asenjo and B. A. Andrews, "Aqueous two-phase systems for protein separation: Phase separation and applications", *Journal of Chromatography A*, vol. 1238, pp. 1-10, 2012.
- [46] F. J. Deive, M. A. Rivas, and A. Rodríguez, "Sodium carbonate as phase promoter in aqueous solutions of imidazolium and pyridinium ionic liquids", *The Journal of Chemical Thermodynamics*, vol. 43, pp. 1153-1158, 2011.
- [47] Z. Li, Y. Pei, H. Wang, J. Fan, and J. Wang, "Ionic liquid-based aqueous two-phase systems and their applications in green separation processes", *TrAC Trends in Analytical Chemistry*, vol. 29, pp. 1336-1346, 2010.
- [48] K. E. Gutowski, G. A. Broker, H. D. Willauer, J. G. Huddleston, R. P. Swatloski, J. D. Holbrey, and R. D. Rogers, "Controlling the Aqueous Miscibility of Ionic Liquids: Aqueous Biphasic Systems of Water-Miscible Ionic Liquids and Water-Structuring Salts for Recycle, Metathesis, and Separations", *Journal of the American Chemical Society*, vol. 125, pp. 6632-6633, 2003.
- [49] F. Hofmeister, *Arch. Exp. Pathol. Pharmacol.*, vol. 24, p. 247-260, 1888.

- [50] A. M. Fernandes, M. A. A. Rocha, M. G. Freire, I. M. Marrucho, J. o. A. P. Coutinho, and L. M. N. B. F. Santos, "Evaluation of Cation–Anion Interaction Strength in Ionic Liquids", *The Journal of Physical Chemistry B*, vol. 115, pp. 4033-4041, 2011.
- [51] S. P. M. Ventura, C. M. S. S. Neves, M. G. Freire, I. M. Marrucho, J. Oliveira, and J. A. P. Coutinho, "Evaluation of anion influence on the formation and extraction capacity of ionic-liquid-based aqueous biphasic systems", *The journal of physical chemistry. B*, vol. 113, pp. 9304-10, 2009.
- [52] Y. Deng, T. Long, D. Zhang, J. Chen, and S. Gan, "Phase Diagram of [Amim]Cl + Salt Aqueous Biphasic Systems and Its Application for [Amim]Cl Recovery", *Journal of Chemical & Engineering Data*, vol. 54, pp. 2470-2473, 2009.
- [53] B. Wu, Y. Zhang, and H. Wang, "Phase Behavior for Ternary Systems Composed of Ionic Liquid + Saccharides + Water", *The Journal of Physical Chemistry B*, vol. 112, pp. 6426-6429, 2008.
- [54] B. Wu, Y. M. Zhang, and H. P. Wang, "Aqueous Biphasic Systems of Hydrophilic Ionic Liquids + Sucrose for Separation", *Journal of Chemical & Engineering Data*, vol. 53, pp. 983-985, 2008.
- [55] A. F. M. Cláudio, A. M. Ferreira, S. Shahriari, M. G. Freire, and J. A. P. Coutinho, "Critical Assessment of the Formation of Ionic-Liquid-Based Aqueous Two-Phase Systems in Acidic Media", *The Journal of Physical Chemistry B*, vol. 115, pp. 11145-11153, 2011.

Appendix

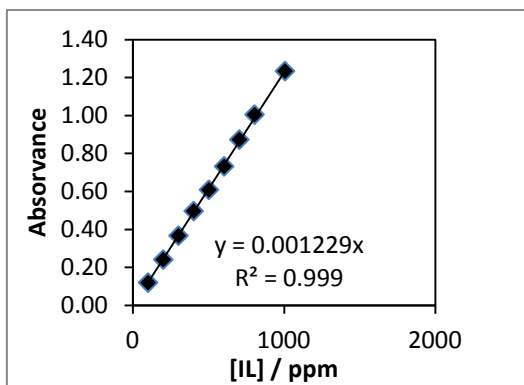
Appendix A

Table A 1 - K_f , n and R^2 values for the Freundlich model. δ stands for standard error associated to each parameter.

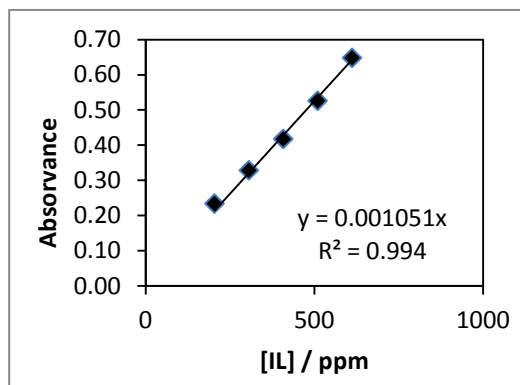
IL	Freundlich		
	$k_f \pm \delta$	$n \pm \delta$	R^2
[C ₁ C ₁ im][NTf ₂]	0.612 ± 0.031	0.465 ± 0.074	0.916
[C ₂ im][NTf ₂]	0.703 ± 0.033	0.450 ± 0.078	0.903
[C ₂ C ₂ im][NTf ₂]	0.694 ± 0.022	0.272 ± 0.039	0.888
[C ₂ C ₃ im][NTf ₂]	0.865 ± 0.024	0.268 ± 0.036	0.951
[C ₃ C ₁ im][NTf ₂]	0.870 ± 0.024	0.227 ± 0.037	0.899
[C ₃ C ₃ im][NTf ₂]	1.070 ± 0.029	0.152 ± 0.027	0.886
[C ₅ C ₁ im][NTf ₂]	0.995 ± 0.015	0.162 ± 0.015	0.964
[C ₆ C ₁ im][NTf ₂]	0.957 ± 0.022	0.161 ± 0.023	0.920

Table A 2 - q_{max} , L and R^2 values for the Langmuir model. δ stands for standard error associated to each parameter.

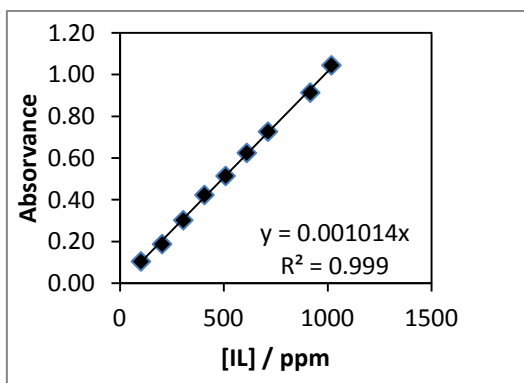
IL	Langmuir		
	$q_{max} \pm \delta$	$L \pm \delta$	R^2
[C ₁ C ₁ im][NTf ₂]	1.104 ± 0.021	1.245 ± 0.136	0.990
[C ₂ im][NTf ₂]	1.376 ± 0.095	1.127 ± 0.215	0.990
[C ₂ C ₂ im][NTf ₂]	0.901 ± 0.016	4.617 ± 0.429	0.991
[C ₂ C ₃ im][NTf ₂]	1.081 ± 0.038	5.307 ± 1.124	0.985
[C ₃ C ₁ im][NTf ₂]	1.027 ± 0.024	6.671 ± 0.933	0.991
[C ₃ C ₃ im][NTf ₂]	1.165 ± 0.007	17.363 ± 1.172	0.998
[C ₅ C ₁ im][NTf ₂]	1.080 ± 0.016	14.910 ± 1.954	0.993
[C ₆ C ₁ im][NTf ₂]	1.023 ± 0.010	15.241 ± 1.329	0.997



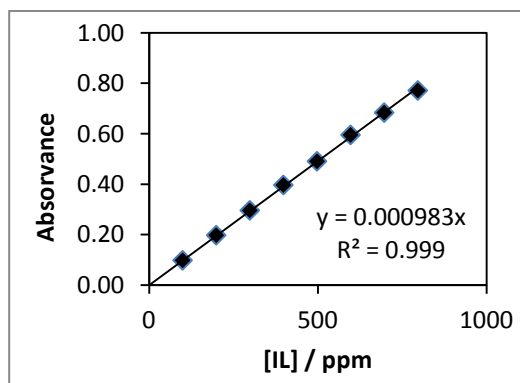
$[C_1C_1im][NTf_2]$



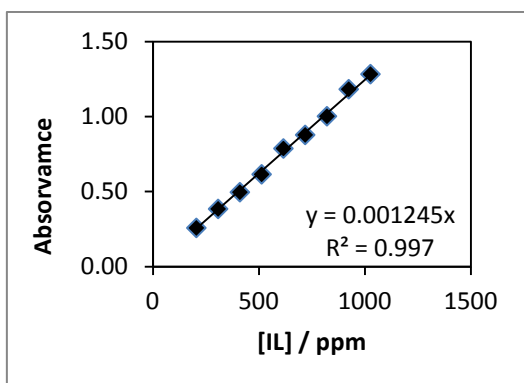
$[C_3C_1im][NTf_2]$



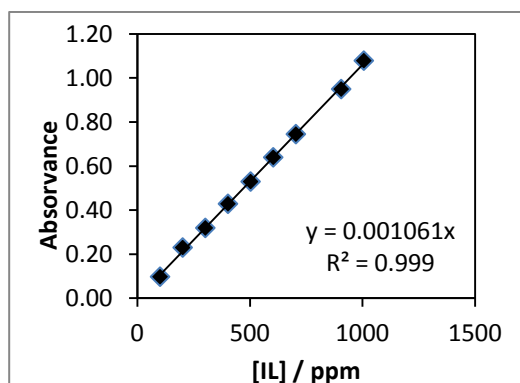
$[C_3C_1im][NTf_2]$



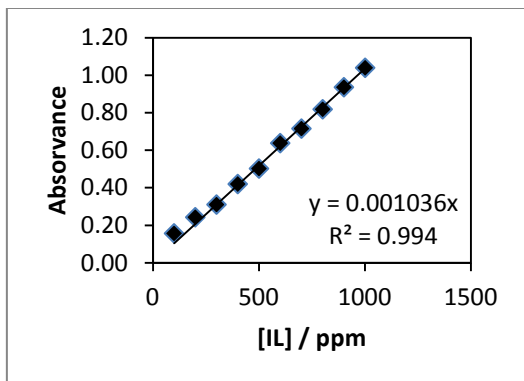
$[C_6C_1im][NTf_2]$



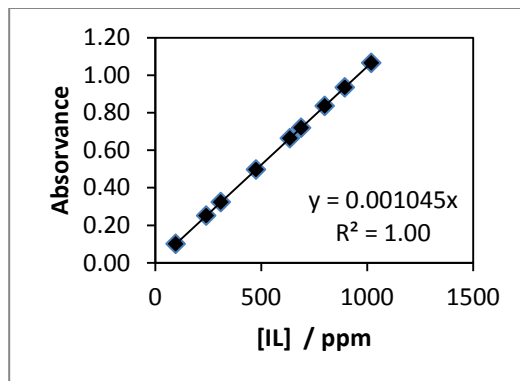
$[C_2im][NTf_2]$



$[C_6C_1im][NTf_2]$



$[C_2im][NTf_2]$



$[C_2C_2im][NTf_2]$

$[C_2C_3im][NTf_2]$

$[C_3C_3im][NTf_2]$

Fig. A 1 - Calibration curves for the ILs studied in this work with the respectively linear fitting and R^2 .

Appendix B

Table B 1 - Experimental binodal curve mass fraction data for the system composed of IL (1) + Na₂CO₃ (2) + H₂O (3) at 298 K.

[C₄C₁im]Cl		M_w = 174.67	
100 w₁	100 w₂	100 w₁	100 w₂
41.5686	2.7448	17.6325	11.1366
33.8129	3.4842	17.1680	11.4377
31.6037	4.1522	16.2135	11.8527
29.7255	4.7229	15.7151	12.2075
27.9213	5.2768	15.2083	12.6092
26.4494	5.7408	14.6020	13.0224
21.6418	8.5535	13.9959	13.4519
21.4602	8.7218	13.5542	13.8842
21.2026	8.8995	12.9253	14.3009
21.0781	9.0387	12.1602	14.8002
20.3252	9.2895	11.3515	15.6770
20.0526	9.4711	10.6257	16.3470
19.6790	9.6508	9.6719	17.0539
19.2390	9.8723	8.9252	17.7982
18.9163	10.1031		
18.6455	10.3356		
18.2303	10.5977		
17.8413	10.8986		

Table B 2 - Experimental binodal curve mass fraction data for the system IL (1) + Na₂CO₃ (2) + H₂O (3) at 298 K.

[C₂C₁im]Cl		M_w= 146.62	
100 w₁	100 w₂	100 w₁	100 w₂
58.1621	0.5449	23.7739	9.0510
43.2543	1.0278	23.3992	9.2199
36.3496	3.0969	23.1941	9.3722
30.0742	5.9579	22.8605	9.5456
29.2963	6.2009	22.5766	9.7070
29.0791	6.3323	22.2625	9.8781
28.7607	6.4846	21.9821	10.0501
28.5368	6.3844	21.6754	10.2341
28.4556	6.6047	21.3036	10.4584
28.3312	6.6822	21.0277	10.6617
28.2079	6.7611	20.7448	10.8603
28.0479	6.8516	20.4352	11.0625
27.9128	6.9386	20.0052	11.3103
27.7806	7.0251	19.5843	11.5615
27.3796	7.1523	19.2051	11.8169
27.2625	7.2413	18.9020	12.0546
26.7946	7.3813	18.4917	12.4315
26.7053	7.4741	18.2259	12.7151
26.5845	7.5777	17.7481	13.0214
26.0754	7.7361	17.3005	13.3389
25.8915	7.8507	16.8326	13.6503
25.7250	7.9661	16.3523	13.9838
25.5799	8.0742	15.8494	14.3573
25.0847	8.2379	15.3462	14.7464
24.8951	8.3615	14.8381	15.1290
24.6583	8.4987	14.2255	15.5546
24.4396	8.6314	13.6655	15.9891
24.2110	8.7724	12.9953	16.4606
23.9741	8.9195	12.5490	16.9691

Table B 3 - Experimental binodal curve mass fraction data for the system IL (1) + Na₂CO₃ (2) + H₂O (3) at 298 K.

[C₆C₁im]Cl		M_w= 202.72	
100 w₁	100 w₂	100 w₁	100 w₂
51.9631	1.1552	22.1725	8.7021
46.5696	1.6040	21.7771	8.8747
44.1993	2.0244	21.1718	8.8555
40.9074	2.4138	21.1564	9.0827
39.0393	2.7794	20.7379	9.2704
37.2520	3.1452	20.4344	9.4383
34.9155	3.8292	19.9834	9.6374
32.2630	4.7190	19.9050	9.7328
29.9768	5.4725	19.4049	9.9256
27.5820	6.3334	18.9767	10.1223
27.1600	6.6150	18.5276	10.3290
26.9253	6.7094	18.0697	10.5530
26.7430	6.8008	17.7611	10.7368
26.4091	6.9149	17.5200	10.9228
26.0746	7.0305	17.0276	11.1548
25.8917	6.8920	16.5305	11.3969
25.6780	7.1575	16.0302	11.6543
25.2601	7.2939	15.9430	11.8042
25.1334	7.3836	15.4073	12.0509
24.8346	7.4986	14.8204	12.3372
24.5929	7.6137	14.6258	12.5607
24.3821	7.7190	13.9231	12.9044
23.9009	7.8720	13.5712	13.1807
23.6805	7.7721	12.5937	13.6105
23.6619	7.9928	12.3417	13.8989
23.2706	8.1419	11.5576	14.3071
23.1002	8.2612	11.2602	14.6194
22.7887	8.4073	10.4316	15.0650
22.4739	8.5526	10.0744	15.4233

Table B 4 - Experimental binodal curve mass fraction data for the system IL (1) + Na₂CO₃ (2) + H₂O (3) at 298 K.

[C₆C₁im]Cl $M_w=202.72$	
100 w_1	100 w_2
9.1793	15.9041
8.4596	16.3870
8.1161	16.7919
7.6115	17.2367
7.1669	17.6511
6.6875	18.0699
6.1569	18.5233
5.6380	18.8011

Table B 5 - Experimental binodal curve mass fraction data for the system IL (1) + Na₂CO₃ (2) + H₂O (3) at 298 K.

[aC_{1im}]Cl		M_w= 158.63	
100 w₁	100 w₂	100 w₁	100 w₂
57.7650	0.6860	22.0392	9.5509
44.3244	1.3435	21.8659	9.6868
41.5280	1.9737	21.5674	9.8472
37.0449	2.9531	21.3929	10.0786
35.0731	3.3812	20.8269	10.3348
32.2436	4.2856	20.5157	10.5142
29.9783	5.8171	20.2642	10.6901
29.0658	6.1272	19.8939	10.9002
28.3057	6.3495	19.5618	11.1167
27.8637	6.5197	19.3779	11.3143
27.6613	6.6255	19.0239	11.5350
27.3301	6.7736	18.6367	11.7706
27.2297	6.8733	18.2162	12.0106
26.9293	6.9815	17.7502	12.2776
26.8099	7.0647	17.4290	12.5353
26.3320	7.2033	16.9876	12.9702
25.9498	7.3809	16.4581	13.3185
25.7244	7.5683	16.1156	13.5958
25.4584	7.7098	15.8327	13.8684
25.0846	7.9048	15.4577	14.1647
24.7244	8.0687	15.0613	14.5014
24.5182	8.1832	13.9495	15.1950
24.3778	8.2886	13.4830	15.6111
23.7753	8.5219	12.8774	16.0337
23.3595	8.7717	12.3378	16.7059
23.0949	8.9468	11.9472	17.1880
22.8368	9.0865		
22.5524	9.2441		
22.3422	9.3855		

Table B 6 - Experimental binodal curve mass fraction data for the system IL (1) + Na₂CO₃ (2) + H₂O (3) at 298 K.

[C₄C₁im]Br		M_w= 219.12	
100 w₁	100 w₂	100 w₁	100 w₂
54.2209	1.0403	25.1323	7.5559
43.5259	1.9326	25.0794	7.6346
40.7441	2.7053	24.7936	7.7474
38.9069	3.0232	24.4843	7.8606
36.7123	3.5645	24.3996	7.9359
34.6201	4.1330	24.0745	8.0517
32.7974	4.6233	23.7818	8.1745
30.6967	5.3405	23.7366	7.9943
29.6785	5.9084	23.4933	8.2982
28.9369	6.1090	23.4091	8.3880
28.8525	5.9602	23.1185	8.5104
28.6895	6.1857	22.7874	8.6320
28.5344	6.2507	22.6845	8.7219
28.2709	6.3293	22.3022	8.8708
28.1514	6.3908	21.9961	9.0123
27.9954	6.4596	21.8626	9.1158
27.9532	6.5134	21.4521	9.2726
27.7712	6.5841	21.0757	9.4302
27.4581	6.6757	20.9641	9.5530
27.2692	6.7493	20.4825	9.7292
27.0218	6.8274	20.3238	9.8454
26.7601	6.9120	19.8410	10.0186
26.6194	6.7931	19.6278	10.1505
26.5169	6.9988	19.3013	10.0365
26.2721	7.0850	19.2336	10.3253
26.0593	7.1737	19.0984	10.4598
25.8182	7.2699	18.5577	10.6761
25.7645	7.3357	18.3669	10.8284
25.4555	7.4433	17.8136	11.0498

Table B 7 - Experimental binodal curve mass fraction data for the system IL (1) + Na₂CO₃ (2) + H₂O (3) at 298 K.

[C ₄ C ₁ im][CF ₃ SO ₃]		<i>M_w</i> =	288.29
100 <i>w</i> ₁	100 <i>w</i> ₂	100 <i>w</i> ₁	100 <i>w</i> ₂
58.9369	0.5251	13.3061	4.6845
46.6759	0.9357	12.8665	4.8088
41.1924	1.3199	12.6119	4.8898
36.7950	1.5719	12.3581	4.9527
33.4487	1.8126	12.1267	5.0106
30.3788	1.9947	11.8316	5.0380
28.2656	2.1829	11.5288	5.1886
26.4296	2.3234	11.2373	5.4466
24.7731	2.4562	10.9951	5.5822
23.4476	2.6361	10.7535	5.7030
22.3581	2.7502	10.5791	5.7388
21.6889	2.8767	10.3457	5.8492
20.9211	2.9976	10.1093	5.9773
20.0825	3.1342	9.8735	6.0971
19.1542	3.2638	9.6516	6.2015
18.3742	3.3627	9.3961	6.3742
17.8552	3.5112	9.1583	6.4113
17.4708	3.5511	8.8820	6.6308
17.0490	3.6614	8.4951	6.8046
16.6749	3.7400	8.2052	7.0313
16.2784	3.8453	7.8085	7.2156
15.9471	3.9148	7.4196	7.4844
15.5332	4.0633	7.0476	7.6781
15.1625	4.1672	6.5897	8.0802
14.7753	4.2657	6.1945	8.4482
14.4170	4.3257	5.9031	8.7237
14.0847	4.3991	5.3406	9.3439
13.8757	4.5048	4.9597	9.7789
13.5659	4.6004	4.6125	10.1868

Table B 8 - Experimental binodal curve mass fraction data for the system IL (1) + Na₂CO₃ (2) + H₂O (3) at 298 K.

[C₄C₁im][CF₃SO₃] M_w=288.29	
100 w₁	100 w₂
4.2332	10.5345
4.0543	10.7645
3.7890	11.0993
3.2141	12.1690
2.3114	14.1020

Table B 9 - Experimental binodal curve mass fraction data for the system IL (1) + Na₂CO₃ (2) + H₂O (3) at 298 K.

[C₄C₁im][Tos]		M_w= 310.41	
100 w₁	100 w₂	100 w₁	100 w₂
57.3652	0.5025	17.7665	7.9328
52.8729	1.0083	17.1123	8.1812
50.2719	1.4740	16.5756	8.3350
46.8319	1.8548	16.1571	8.4741
43.8677	2.1973	15.8679	8.5062
41.2055	2.5384	15.5303	8.6788
39.5563	2.8726	15.2691	8.7066
37.9644	3.1765	14.8557	8.8412
36.5667	3.4404	14.5043	8.9444
35.2517	3.7086	14.0640	9.1129
34.0685	3.9617	13.7777	9.2001
32.8756	4.2070	13.4321	9.2895
31.7533	4.4290	13.1092	9.3899
30.6989	4.6457	12.8118	9.5103
29.6873	4.8315	12.5396	9.5941
28.7210	5.0308	12.2040	9.7272
27.8568	5.2428	11.9233	9.8289
27.0347	5.4084	11.6630	9.9175
25.8563	5.7380	11.3803	10.0240
24.8234	6.0458	11.1197	10.1295
24.0312	6.2520	10.9098	10.1967
23.5112	6.3953	10.7066	10.2677
22.8714	6.4770	10.4937	10.3212
21.9371	6.7994	10.1962	10.4561
21.3760	6.8994	9.9446	10.5771
20.8126	6.9828	9.7530	10.6417
19.8566	7.3520	9.5732	10.7011
19.1461	7.6070	9.3527	10.8048
18.7196	7.6718	9.1326	10.9120
18.1262	7.8599	8.9117	11.0122

Table B 10 - Experimental binodal curve mass fraction data for the system IL (1) + Na₂CO₃ (2) + H₂O (3) at 298 K.

[C₄C₁im][N(CN)₂]		M_w= 205.26	
100 w₁	100 w₂	100 w₁	100 w₂
58.1355	0.5314	3.7075	13.9382
46.3029	1.0808	3.2060	14.6330
43.0437	1.5243		
39.3171	1.9075		
36.8240	2.2299		
35.2820	2.6118		
33.4039	2.9138		
31.5455	3.1914		
30.4086	3.5053		
29.0804	3.7255		
28.0708	3.9743		
27.1252	4.2167		
25.9573	4.3788		
25.2356	4.5768		
24.1137	4.9603		
11.6377	8.3191		
10.9585	8.4131		
10.3874	8.6958		
9.9456	8.9195		
8.6763	9.5047		
8.2716	9.6982		
7.0401	10.9784		
6.4002	11.3677		
6.0076	11.7067		
5.7014	11.9091		
5.3682	12.1738		
5.0286	12.4841		
4.6106	12.9570		
4.2774	13.3195		
4.0067	13.6105		

Table B 11 - Experimental binodal curve mass fraction data for the system IL (1) + Na₂CO₃ (2) + H₂O (3) at 298 K.

[C₄C₁im][CH₃SO₄]		M_w= 250.31	
100 w₁	100 w₂	100 w₁	100 w₂
58.3891	0.6235	9.3208	15.3280
51.8037	1.1862	8.6768	15.9816
47.2774	1.6513	6.9578	16.9676
44.5902	2.1058	6.0643	17.8269
42.2038	2.5064	5.2666	18.6825
39.4376	2.7865		
36.7473	3.5306		
34.2947	4.2091		
32.1816	4.7978		
30.2834	5.2988		
27.1611	6.4613		
25.3860	7.3928		
24.6929	7.6518		
24.0892	7.6839		
23.8875	7.9413		
23.0976	8.2541		
22.7187	8.5059		
21.7896	8.8399		
21.1986	9.1483		
20.0978	9.5335		
20.0140	9.5075		
19.2806	9.9064		
18.7416	10.2303		
17.4138	10.7167		
16.5185	11.1740		
16.0771	11.3784		
14.6286	12.4267		
13.4974	13.0855		
12.2575	13.7570		
10.8772	14.4752		

Table B 12 - Experimental binodal curve mass fraction data for the system IL (1) + Na₂CO₃ (2) + H₂O (3) at 298 K.

[C₄C₁im][C₂H₅SO₄] <i>M_w</i>=264.34	
100 <i>w</i>₁	100 <i>w</i>₂
56.0389	1.3267
46.4982	1.8268
42.7100	2.2663
42.3962	2.3461
40.4017	2.7351
39.8626	2.8412
38.2985	3.1658
37.5963	3.2923
36.3380	3.6025
35.6026	3.6550
34.6297	3.9434
33.7541	4.0097
33.0694	4.2463
31.6452	4.5088
31.3679	4.7005
29.4695	5.2065
29.1288	5.3571
27.4429	5.8683
25.0642	6.7764
23.0263	7.5406
20.9146	8.3904
18.6279	9.4119
16.6004	10.3254
15.0900	10.9978

Table B 13 - Experimental binodal curve mass fraction data for the system IL (1) + Na₂CO₃ (2) + H₂O (3) at 298 K.

[C₄C₁im][CH₃SO₃]		M_w= 234.32	
100 w₁	100 w₂	100 w₁	100 w₂
59.8275	0.8609	9.6110	17.4998
51.1588	1.5589		
46.4396	2.1021		
41.1512	3.0933		
38.9643	3.5091		
35.2406	4.1796		
29.0885	6.5779		
28.6078	6.7650		
28.0315	6.9753		
27.4624	7.2021		
27.2356	7.3840		
26.6466	7.6229		
25.6137	7.9427		
24.8803	8.2496		
24.4730	8.5130		
24.0387	8.7897		
23.5263	9.0822		
22.9153	9.3990		
21.8185	9.8402		
21.2968	10.1957		
20.0177	10.7019		
19.2782	11.1303		
18.4369	11.6393		
17.6831	12.1221		
16.7535	12.6871		
15.6861	13.3252		
14.4370	14.0348		
13.1331	14.8093		
11.6447	15.6779		
10.9920	16.4220		

Table B 14 - Experimental binodal curve mass fraction data for the system IL (1) + Na₂CO₃ (2) + H₂O (3) at 298 K.

[C₄C₁im][DMP] $M_w=264.26$	
100 w_1	100 w_2
51.0129	2.1654
39.0398	3.1601
30.4151	5.7636
26.1655	8.1431
25.1673	8.6170
24.5557	8.9799
23.7187	9.3166
22.8384	9.7203
21.7289	10.1420
20.7462	10.5989
20.3837	10.9228
19.7759	11.2644
18.9063	11.7658
17.9718	12.3480
16.3242	13.0001
15.8280	13.3776
15.1060	13.8780
14.8047	14.2688
14.1880	14.6226
13.7644	14.9138
13.2904	15.2268
12.8028	15.8362
12.4509	16.8557

Table B 15 - Experimental binodal curve mass fraction data for the system IL (1) + Na₂CO₃ (2) + H₂O (3) at 298 K.

[C ₄ C ₁ im][SCN]		$M_w = 194.28$	
100 w_1	100 w_2	100 w_1	100 w_2
57.9075	0.6895	13.2912	6.5732
45.1559	1.2152	12.9852	6.6164
40.7561	1.7310	12.5707	6.7694
37.0598	2.1233	12.1637	6.9182
34.6914	2.4560	11.9797	6.9772
32.6315	2.7802	11.6512	7.0721
30.8838	3.0285	11.4758	7.1383
29.2392	3.2959	11.3162	7.1911
28.1632	3.5803	11.1235	7.2818
26.8227	3.7867	10.8863	7.2945
25.6083	3.9339	10.5895	7.4079
24.4904	4.0842	10.3153	7.5033
23.8002	4.2951	10.0514	7.5996
22.8518	4.4340	9.8008	7.7173
22.0041	4.5935	9.4608	7.8675
21.4721	4.7324	9.2180	7.9593
20.6338	4.8335	9.0053	8.0322
20.0719	5.0181	8.7019	8.1469
19.3236	5.1156	8.4585	8.2771
18.8838	5.2572	8.2192	8.4224
17.0508	5.6959	7.9605	8.4982
16.6720	5.8164	7.7137	8.6770
16.1487	5.8649	7.4217	8.7826
15.8101	5.9925	7.1263	8.9695
15.3753	6.0378	6.7841	9.0885
15.0651	6.1277	3.4462	10.6489
14.7718	6.2273	2.7371	12.3003
14.3945	6.2659	2.4921	13.2349
14.1381	6.3525	2.0324	15.0699
13.8845	6.4362	1.4917	16.4997
13.6425	6.5249	1.0236	19.6763

Table B 16 - Experimental binodal curve mass fraction data for the system IL (1) + Na₂CO₃ (2) + H₂O (3) at 298 K.

[C₄-3-C₁py]Cl		M_w= 185.69	
100 w₁	100 w₂	100 w₁	100 w₂
56.2081	0.8846	16.5580	10.7305
41.6454	1.2888	16.3970	10.8411
38.5337	1.6651	16.2196	10.9593
37.0468	2.0491	16.0230	11.0881
34.6989	2.6609	15.8528	11.2134
33.4089	2.9973	15.6890	11.3428
32.2252	3.2756	15.5143	11.4733
30.5617	3.8431	15.3299	11.6063
29.6218	4.0646	15.1140	11.7493
28.6643	4.2657	14.9152	11.8959
27.3171	4.7263	14.6846	12.0472
25.1615	5.6572	14.4537	12.2114
23.4561	6.4519	14.2091	12.3809
21.9098	7.1103	13.9706	12.5514
19.6915	8.1865	13.7079	12.7209
19.0764	9.1472	13.4281	12.8985
19.0114	9.2288	13.1329	13.0874
18.8732	9.3143	12.8431	13.2647
18.7255	9.4059	12.5416	13.4669
18.6114	9.4973	12.2796	13.6630
18.2784	9.6247	11.9587	13.8727
18.1490	9.7216	11.6249	14.0849
18.0084	9.8261	11.3075	14.4289
17.8938	9.9282	11.0510	14.6518
17.7794	10.0265	10.4745	14.8916
17.6418	10.1356	10.0744	15.1173
17.2348	10.2865	9.6923	15.5041
17.0656	10.3975	9.2803	15.8043
16.8832	10.5111	8.8477	16.2844
16.7133	10.6191	8.4708	16.5985

Table B 17 - Experimental binodal curve mass fraction data for the system IL (1) + Na₂CO₃ (2) + H₂O (3) at 298 K.

[C₄-3-C₁py]Cl $M_w=185.69$	
100 w_1	100 w_2
7.9672	16.9234
7.4902	17.4310
7.0548	18.0024
6.7347	18.3645

Table B 18 - Experimental binodal curve mass fraction data for the system IL (1) + Na₂CO₃ (2) + H₂O (3) at 298 K.

[C₄py]Cl		M_w= 171.67	
100 w₁	100 w₂	100 w₁	100 w₂
60.3807	0.5159	23.8911	9.0427
46.4581	1.0776	23.7725	9.1759
42.5713	1.5573	23.3254	9.3631
39.4147	2.4265	23.1760	9.5043
37.6484	2.7654	23.0351	9.6460
36.0202	3.0815	22.9026	9.7866
33.7762	3.7314	22.3869	10.0070
31.2451	4.6057	22.2584	10.1751
28.5852	6.3714	22.1206	10.3455
28.5633	6.4333	21.6052	10.5935
28.3029	6.5321	21.4299	10.7818
28.0551	6.6317	21.2357	10.9630
27.8287	6.7290	21.0627	11.1233
27.5805	6.8267	20.8255	11.3160
27.2509	6.9729	20.2251	11.7471
27.1492	7.0797	19.8125	12.0627
27.1023	7.1623	19.5319	12.3200
26.8283	7.2729	19.3639	12.5511
26.4860	7.3948	19.1444	12.8100
26.2214	7.5108	18.4625	13.1898
26.1471	7.6020	18.1896	13.4811
26.0696	7.6970	17.8395	13.7910
25.7605	7.8320	17.4824	14.1134
25.7018	7.9327	17.1838	14.4191
25.3513	8.0783	17.0045	14.7383
25.2755	8.1863	16.6202	15.1036
24.9095	8.3498	16.1866	15.5066
24.4138	8.7335	15.9398	15.9135
24.2946	8.6203		
23.9808	8.9154		

Table B 19 - Experimental binodal curve mass fraction data for the system IL (1) + Na₂CO₃ (2) + H₂O (3) at 298 K.

[C₄-2-C₁py]Cl		M_w= 185.69	
100 w₁	100 w₂	100 w₁	100 w₂
63.7669	0.3556	14.9754	12.5163
30.1776	4.6640	14.1903	12.8797
24.6639	6.7608	13.7878	13.1821
24.2190	7.1107	13.4419	13.4501
23.5743	7.3425	13.0118	13.7715
23.3893	7.4837	12.6171	14.0382
22.5997	7.7468	12.1374	14.3911
22.4017	7.9537	11.6653	14.7715
22.1650	8.1104	11.3295	15.0794
21.7586	8.2695	10.6932	15.5184
21.2235	8.4533	10.1840	15.8998
21.0350	8.5870	9.5924	16.5630
20.8714	8.7232	9.1541	17.0331
20.7491	8.8566	8.4683	17.5447
20.2630	9.0528	8.0010	17.9494
19.7290	9.2630		
19.5580	9.4125		
19.3812	9.5732		
18.7811	9.8081		
18.5175	9.9942		
18.2942	10.1857		
18.0844	10.3767		
17.8723	10.5602		
17.1282	10.8460		
16.9061	11.0442		
16.6626	11.2470		
16.3429	11.4840		
16.0616	11.7132		
15.6953	11.9640		
15.3708	12.2241		

Table B 20 - Experimental binodal curve mass fraction data for the system IL (1) + Na₂CO₃ (2) + H₂O (3) at 298 K.

[C₄-4-C₁py]Cl		M_w= 185.69	
100 w₁	100 w₂	100 w₁	100 w₂
59.3893	0.6654	16.1045	10.7507
37.5270	2.1793	15.9268	10.9026
34.0812	2.9432	15.6876	11.0775
31.8277	3.6978	15.1384	11.3068
30.0505	4.3694	14.9699	11.4697
28.3541	4.8991	14.7429	11.6441
26.9025	5.3706	14.5555	11.8199
25.1440	6.1544	13.9795	12.0782
23.6540	6.7862	13.8045	12.2556
22.5151	7.2672	13.5681	12.4465
21.3965	7.8440	12.9952	12.7231
21.1233	7.9558	12.7759	12.9372
20.9008	8.0646	12.5444	13.1724
20.8190	8.1544	11.8892	13.4720
20.5836	8.1467	11.6416	13.7119
20.2800	8.3706	11.3146	13.9732
20.0874	8.5002	10.9831	14.2503
19.9736	8.5916	10.6769	14.5406
19.6353	8.7186	9.9222	14.9232
19.2376	8.8604	9.5742	15.2235
19.1126	8.9727	9.1898	15.5626
18.8094	9.1123	8.8601	15.8789
18.4568	9.2663	8.4083	16.2365
18.1156	9.4817	8.0900	16.5971
17.7292	9.7505	7.6586	16.9936
17.5093	9.9213	7.2854	17.4031
17.0808	10.0958	6.8035	17.8359
16.8710	10.2431	6.0758	18.3095
16.7214	10.3917	5.5163	18.7045
16.5875	10.5432	5.1449	19.5036

Table B 21 - Experimental binodal curve mass fraction data for the system IL (1) + Na₂CO₃ (2) + H₂O (3) at 298 K.

[C₄C₁pyr]Cl		M_w= 177.67	
100 w₁	100 w₂	100 w₁	100 w₂
57.2710	0.6677	15.9521	10.9866
42.0388	1.2456	15.7234	11.1444
38.7186	1.7743	15.4819	11.2932
36.2218	2.1582	15.2470	11.4543
33.9483	2.5152	15.0595	11.6139
31.7579	3.2773	14.8015	11.7946
30.4179	3.6070	14.5217	11.9832
27.8774	4.6576	14.1866	12.1833
26.3457	5.1840	13.9047	12.3955
23.5177	6.5046	13.7012	12.5956
21.3166	7.6749	13.1869	12.8653
21.0873	7.8317	12.8093	13.2586
20.7691	8.0144	12.5866	13.4988
20.5548	7.9393	12.2974	13.7546
20.4384	8.2121	11.9272	14.0528
20.1549	8.4017	11.5863	14.3371
19.8258	8.5533	11.1795	14.6211
19.3682	8.7787	10.7772	14.9166
19.0999	8.9715	10.4546	15.1984
18.7665	9.1266	9.9933	15.5387
18.5906	9.2550	9.4799	15.8870
18.2699	9.3957	8.9781	16.4428
18.0567	9.5664	8.5932	16.8253
17.6474	9.7995	8.0748	17.2306
17.5075	9.9461	7.6605	17.6377
17.0782	10.1272	7.2668	18.1186
16.8399	10.2699		
16.5736	10.4156		
16.3039	10.6531		
16.1912	10.8160		

Table B 22 - Experimental binodal curve mass fraction data for the system IL (1) + Na₂CO₃ (2) + H₂O (3) at 298 K.

[C₄C₁pip]Cl		M_w= 191.74	
100 w₁	100 w₂	100 w₁	100 w₂
57.3892	0.5965	16.5394	9.7598
43.9336	1.1273	16.1453	9.9127
40.0358	1.5936	15.9879	10.1186
37.8301	2.0046	15.7272	10.3073
35.1974	2.3369	15.2818	10.4845
33.9188	2.6835	15.0227	10.6862
32.1110	2.9817	14.8384	10.8320
30.4262	3.6446	14.5432	10.9815
29.4540	3.9120	14.2925	11.1991
28.4693	4.1812	14.0716	11.3994
27.2144	4.6936	13.8041	11.5749
26.5627	4.8681	13.5669	11.7539
25.4491	5.3099	13.3288	11.9171
24.4296	5.6984	13.0050	12.0700
23.0925	6.2964	12.8512	12.2357
22.1573	6.6621	12.6111	12.4159
19.4026	8.1856	12.3788	12.5794
18.6861	8.4534	12.0724	12.7672
18.5090	8.5487	11.7601	13.0708
18.3507	8.6491	11.5429	13.2757
18.2778	8.7262	11.2340	13.4946
18.0896	8.8235	10.7470	13.8310
17.9026	8.9220	10.4350	14.0724
17.7717	9.0146	10.1539	14.2973
17.6174	9.1163	9.8822	14.5259
17.3717	9.2375	9.4966	14.7914
17.2644	9.3314	9.1234	15.0480
17.0721	9.4377	8.9219	15.3248
16.8661	9.5510	8.5760	15.5763
16.7294	9.6481	8.2461	15.8102

Table B 23 - Experimental binodal curve mass fraction data for the system IL (1) + Na₂CO₃ (2) + H₂O (3) at 298 K.

[C₄C₁pip]Cl $M_w=191.74$	
100 w_1	100 w_2
7.9015	16.2272
7.5387	16.6760
6.7983	17.3018
6.4164	17.6106
5.9291	17.9710
5.4617	18.6176

Table B 24 - Experimental binodal curve mass fraction data for the system IL (1) + Na₂CO₃ (2) + H₂O (3) at 298 K.

[P₄₄₄₄]Cl		M_w= 294.88	
100 w₁	100 w₂	100 w₁	100 w₂
60.7523	1.9068	15.2861	8.0819
41.3556	2.2216	14.9149	8.2326
37.7082	2.4946	14.4381	8.4894
35.4922	2.7846	14.1245	8.6219
33.6446	3.0418	13.8031	8.7601
31.9861	3.2467	13.4835	8.8796
30.9537	3.4944	13.1091	9.0689
29.9555	3.7559	12.7357	9.2495
28.5056	3.9148	12.3897	9.4512
27.6154	4.1249	12.1398	9.5484
26.8477	4.2914	11.8282	9.7237
25.7737	4.6964	11.5604	9.8708
25.0893	4.8608	11.3496	9.9399
24.4108	5.0198	11.0635	10.0908
23.8240	4.9600	10.8020	10.2402
23.2140	5.1198	10.5685	10.3717
22.3819	5.4364	10.3439	10.4978
21.8403	5.5659	10.1705	10.5644
21.3386	5.7029	9.9454	10.6853
20.6366	5.9980	9.7518	10.7882
20.1724	6.1118	9.5547	10.9112
19.5351	6.3894	9.3659	11.0128
19.1279	6.4848	9.1722	11.1128
18.5365	6.7364	8.9981	11.2187
17.9923	6.9601	8.8243	11.3158
17.4806	7.1772	8.6627	11.4089
17.0242	7.3579		
16.5521	7.5420		
16.1125	7.7398		
15.6875	7.9208		

Table B 25 - Experimental binodal curve mass fraction data for the system IL (1) + Na₂CO₃ (2) + H₂O (3) at 298 K.

[N₄₄₄₄]Cl		M_w= 277.92	
100 w₁	100 w₂	100 w₁	100 w₂
58.8850	0.5968	8.3468	12.1941
39.9871	1.1155	7.8466	12.5542
36.7647	1.5685	7.4055	12.8577
33.9206	1.9281	7.0279	13.1199
32.3034	2.2888	6.6225	13.4300
30.9335	2.6283	6.2567	13.7005
29.5759	2.9303	5.8475	14.0382
28.3416	3.2182	5.4426	14.3807
27.3598	3.4561	5.1708	14.5771
25.9057	3.9552	4.8142	14.8920
24.9929	4.1538		
23.7057	4.6128		
22.9197	4.7803		
21.8695	5.1699		
20.9142	5.4789		
19.7226	6.0179		
18.7226	6.4288		
17.5324	7.0040		
16.6922	7.3718		
15.7532	7.8308		
14.8749	8.3040		
13.9646	8.7926		
13.1666	9.2480		
12.4663	9.6199		
11.5631	10.2105		
11.0258	10.5017		
10.3802	10.9099		
9.7538	11.3169		
9.2665	11.6153		
8.8193	11.8931		

Table B 26 - Values of the parameters of the fitting by the Merchuck equation and R^2 for all the systems investigated. δ stands for the standard error associated to each parameter.

IL + Na₂CO₃ + H₂O	A ± δ	B ± δ	C ± δ	R²
[C ₄ C ₁ im]Cl	67.400 ± 1.055	-0.372 ± 0.007	8.09E-05 ± 3.99E-06	0.999
[C ₄ C ₁ im]Br	78.000 ± 0.618	-0.390 ± 0.004	1.00E-04 ± 3.24E-06	0.999
[C ₄ C ₁ im][CF ₃ SO ₃]	126.000 ± 2.569	-1.026 ± 0.017	4.00E-04 ± 2.00E-04	0.996
[C ₄ C ₁ im][Tos]	80.052 ± 0.834	-0.413 ± 0.007	7.00E-04 ± 1.65E-05	0.998
[C ₄ C ₁ im][N(CN) ₂]	85.994 ± 1.713	-0.555 ± 0.013	5.00E-04 ± 3.57E-05	0.996
[C ₄ C ₁ im][CH ₃ SO ₄]	80.225 ± 0.475	-0.408 ± 0.003	1.00E-04 ± 4.36E-06	0.999
[C ₄ C ₁ im][CH ₃ SO ₃]	86.390 ± 0.803	-0.417 ± 0.050	8.10E-05 ± 5.56E-06	0.999
[C ₄ C ₁ im][DMP]	72.493 ± 2.509	-0.346 ± 0.014	9.37E-05 ± 8.69E-06	0.995
[C ₄ C ₁ im][C ₂ H ₅ SO ₄]	96.999 ± 3.059	-0.521 ± 0.019	6.67E-05 ± 4.28E-05	0.997
[C ₄ C ₁ im][SCN]	97.714 ± 1.716	-0.653 ± 0.012	1.00E-03 ± 5.02E-05	0.997
[C ₄ C ₁ pip]Cl	75.417 ± 1.181	-0.468 ± 0.009	7.90E-05 ± 8.87E-06	0.994

Table B 27 - Values of the parameters of the fitting by the Merchuck equation and R^2 for all the systems investigated. δ stands for the standard error associated to each parameter.

IL + Na₂CO₃ + H₂O	A ± δ	B ± δ	C ± δ	R²
[C ₄ C ₁ pyr]Cl	63.834±0.305	-0.382 ± 0.002	9.16E-05 ± 2.03E-06	0.999
[C ₄ py]Cl	64.142±0.368	-0.321 ± 0.003	3.16E-05 ± 2.44E-06	0.999
[C ₄ -3-C ₁ py]Cl	62.636±0.449	-0.367 ± 0.003	1.00E-04 ± 1.91E-06	0.999
[C ₄ -2-C ₁ py]Cl	83.399±0.441	-0.456 ± 0.003	6.45E-05 ± 2.70E-06	0.999
[C ₄ -4-C ₁ py]Cl	67.568±0.449	-0.391 ± 0.003	1.00E-04 ± 1.91E-06	0.999
[C ₂ C ₁ im]Cl	58.059±0.612	-0.271 ± 0.004	9.39E-05 ± 3.24E-06	0.997
[C ₆ C ₁ im]Cl	77.643±0.520	-0.398 ± 0.003	1.00E-04 ± 3.12E-06	0.999
[aC ₁ im]Cl	65.261±0.471	-0.328 ± 0.003	7.46E-05 ± 2.65E-06	0.999
[P ₄₄₄₄]Cl	106.911±1.685	-0.655 ± 0.008	2.00E-04 ± 1.30E-05	0.999
[N ₄₄₄₄]Cl	65.723±0.319	-0.467 ± 0.003	2.00E-04 ± 3.84E-06	0.999

Table B 28 - Weight fraction of the phase forming components in the several systems at 298 K, and respective values of α and TLL.

IL	weight fraction composition / wt %							
	[IL] _T	[Salt] _T	[IL] _M	[Salt] _M	[IL] _B	[Salt] _B	α	TLL
[C ₄ C ₁ im]Cl	28.98	5.01	20.23	11.93	2.44	25.98	0.67	33.82
	33.80	3.40	21.12	12.77	2.03	26.88	0.60	39.50
[C ₂ C ₁ im]Cl	33.27	4.11	25.04	11.06	0.64	31.68	0.75	42.72
	43.36	1.16	29.97	12.93	0.04	39.26	0.69	57.69
[C ₆ C ₁ im]Cl	35.26	3.87	25.64	9.96	2.40	24.66	0.71	38.89
	38.75	3.02	26.06	10.81	1.92	25.63	0.66	43.22
[aC ₁ im]Cl	34.22	3.83	25.58	9.94	3.65	25.45	0.72	37.45
[C ₄ C ₁ im]Br	35.04	4.13	26.01	9.19	5.38	20.76	0.70	34.00
	35.04	4.13	25.90	11.31	3.23	23.47	0.58	44.53
[C ₄ C ₁ im][CF ₃ SO ₃]	34.45	1.61	26.93	3.37	4.98	8.51	0.74	30.27
	37.37	1.42	27.11	4.05	3.15	10.19	0.70	35.32
[C ₄ C ₁ im][Tos]	43.88	2.08	30.06	6.12	2.18	14.29	0.67	43.46
	46.23	1.74	30.16	7.03	0.54	16.77	0.65	48.09
[C ₄ C ₁ im][N(CN) ₂]	44.16	1.43	22.30	8.00	2.90	13.84	0.47	43.09
	60.08	0.42	30.01	10.08	0.16	19.67	0.50	62.93
[C ₄ C ₁ im][CH ₃ SO ₄]	39.47	3.00	30.12	8.01	4.16	21.91	0.74	40.06
	54.43	0.91	34.81	12.04	0.35	31.60	0.64	62.19
[C ₄ C ₁ im][C ₂ H ₅ SO ₄]	38.23	3.17	26.69	9.30	4.88	20.88	0.65	37.76
	46.69	1.96	29.95	10.01	3.76	22.61	0.61	47.64
[C ₄ C ₁ im][CH ₃ SO ₃]	39.28	3.55	29.96	8.98	3.33	24.51	0.74	41.61
[C ₄ C ₁ im][DMP]	29.45	6.41	21.96	12.09	1.70	27.46	0.73	34.83
	34.40	4.53	24.02	14.03	0.12	35.90	0.70	47.64
[C ₄ C ₁ im][SCN]	41.64	1.69	20.53	6.06	6.97	8.86	0.39	35.40
	47.35	1.22	20.44	7.11	3.09	10.90	0.39	45.31
[C ₄ py]Cl	32.88	4.31	26.19	10.01	6.83	26.51	0.74	34.22
	39.28	2.33	29.59	12.22	0.84	41.57	0.75	54.93
[C ₄ -3-C ₁ py]Cl	27.01	5.08	20.80	9.95	2.39	24.39	0.75	31.29
	30.54	3.77	21.18	10.91	1.77	25.73	0.67	36.20
[C ₄ -2-C ₁ py]Cl	27.48	5.79	21.94	9.97	3.92	23.57	0.76	29.72
	31.15	4.61	22.27	11.08	3.06	25.10	0.68	34.62
[C ₄ -4-C ₁ py]Cl	26.71	5.43	20.32	9.87	4.65	20.74	0.71	26.85
	29.55	4.37	19.92	11.19	2.94	23.20	0.64	32.59
[C ₄ C ₁ pyr]Cl	31.87	3.27	25.87	8.18	0.97	28.60	0.81	39.95
	33.19	2.90	26.13	9.09	0.42	31.59	0.78	43.56
[C ₄ C ₁ pip]Cl	32.95	3.11	26.86	7.31	2.53	24.06	0.80	39.36
	36.09	2.47	25.89	9.86	1.18	27.77	0.71	43.11
[P ₄₄₄₄]Cl	30.73	3.57	25.20	6.06	3.57	15.82	0.80	29.79
	35.11	2.86	25.70	7.15	2.14	17.87	0.71	36.23
[N ₄₄₄₄]Cl	30.15	2.76	20.86	8.25	1.91	19.47	0.67	32.81
	31.68	2.42	20.32	9.22	1.41	20.52	0.62	35.27

Table B 29 - Weight of the IL- and salt-rich phases and respective TL number.

IL	m_{salt} / g	m_{IL} / g	TL number
[C ₄ C ₁ im]Cl	1.6035	3.3820	1
	2.0119	3.0638	2
[C ₂ C ₁ im]Cl	1.1670	3.7638	1
	1.1642	3.4628	2
[C ₆ C ₁ im]Cl	1.4047	3.6163	1
	1.7043	3.3453	2
[aC ₁ im]Cl	1.2869	3.6395	1
[C ₄ C ₁ im]Br	1.4372	3.4985	1
	2.0782	2.9019	2
[C ₄ C ₁ im][CF ₃ SO ₃]	1.0287	3.7492	1
	1.2554	3.5143	2
[C ₄ C ₁ im][Tos]	1.6432	3.3635	1
	1.6457	3.2511	2
[C ₄ C ₁ im][N(CN) ₂]	2.6060	2.3605	1
	2.7174	2.9948	2
[C ₄ C ₁ im][CH ₃ SO ₄]	1.2753	3.6843	1
	1.7756	3.2122	2
[C ₄ C ₁ im][C ₂ H ₅ SO ₄]	2.0249	3.2964	1
	1.9854	3.6633	2
[C ₄ C ₁ im][CH ₃ SO ₃]	1.2554	3.7207	1
[C ₄ C ₁ im][DMP]	1.3202	3.6721	1
	1.6702	3.5127	2
[C ₄ C ₁ im][SCN]	1.2109	1.9316	1
	2.9772	1.9297	2
[C ₄ py]Cl	1.2615	3.7295	1
	1.5727	3.7778	2
[C ₄ -3-C ₁ py]Cl	1.1496	3.7387	1
	1.0961	3.3761	2
[C ₄ -2-C ₁ py]Cl	1.1864	3.8262	1
	1.5020	3.4380	2
[C ₄ -4-C ₁ py]Cl	1.3894	3.5719	1
	1.7362	3.1928	2
[C ₄ C ₁ pyr]Cl	0.9045	4.0418	1
	1.0383	3.9287	2
[C ₄ C ₁ pip]Cl	1.3546	3.5524	1
	0.9910	4.0912	2
[P ₄₄₄₄]Cl	0.9716	3.9981	1
	1.4490	3.6331	2
[N ₄₄₄₄]Cl	1.6347	3.4152	1
	1.8513	3.1542	2